AD-A165 008 LASER METALWORKING TECHNOLOGY TRANSFER(U) AVCO EVERETT 1/1
RESEARCH LAB INC EVERETT MA O A SANDVEN 1986
N00014-82-C-2373

UNCLASSIFIED F/G 11/6 NL

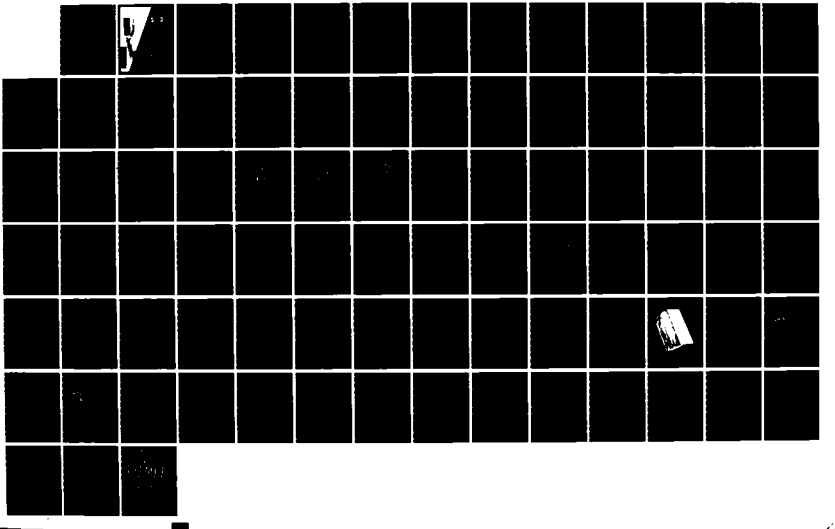

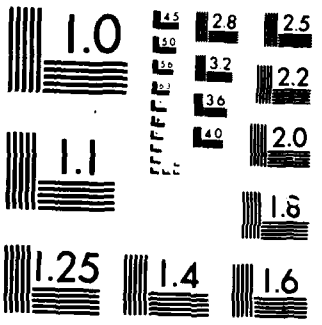

MICROCOPY RESOLUTION TEST CHART

LASER METALWORKING TECHNOLOGY TRANSFER FINAL REPORT

Contract N00014-82-C-2373

prepared for

THE NAVAL RESEARCH LABORATORY
Washington, DC 20375

by

Ole A. Sanden

AVCO EVERETT RESEARCH LABORATORY, INC.
A SUBSIDIARY OF AVCO CORPORATION

2385 REVERE BEACH PARKWAY
EVERETT, MA 02149

LASER METALWORKING TECHNOLOGY TRANSFER

FINAL REPORT

Contract N00014-82-C-2373

prepared for

THE NAVAL RESEARCH LABORATORY

Washington, DC 20375

by

Ole A. Sandven

Avco Everett Research Laboratory, Inc.
a Subsidiary of Avco Corporation
2385 Revere Beach Parkway
Everett, MA 02149

TABLE OF CONTENTS

TABLE OF CONTENTS

(cont.)

LIST OF ILLUSTRATIONS

LIST OF ILLUSTRATIONS
(cont.)

LIST OF TABLES

1. INTRODUCTION

The object of the Technology Transfer Program is to assist in the utilization and integration of the laser facility at FMC/NOD into the manufacturing processes of naval ordnance components and systems.

This assistance consists of targeting workpieces and production steps suitable for laser processing in terms of cost effectiveness and quality enhancement, the development of techniques and procedures for such processing and the establishment of processing parameters and other pertinent data.

The work performed under this program has mainly been related to laser surface transformation hardening of steels. The response of a number of frequently used steels to such laser processing has been determined over a wide range of processing parameters, models, and calculator programs for the prediction of laser hardening have been developed and tested, and the necessary thermophysical constants of the various materials determined by statistical and empirical means.

In addition to the transformation hardening survey, process development work relating to the laser hardfacing of aircraft carrier catapult rails have been performed, and preliminary techniques and processing data established for different combinations of hardfacing alloys/substrate materials.

All the laser processing performed in this program was carried out at Avco Everett Metalworking Laser facilities in Somerville, MA. An Avco HPL®-10 CO_2 laser with constant wave output was used throughout. Analysis of processing results was also done at AEML with the exception of some metallography and microhardness survey performed at FMC/NOD.

2. LASER SURFACE TRANSFORMATION HARDENING

2.1 General Considerations

2.1.1. The Process

Laser surface transformation hardening is a relatively new process, made possible by the development of high powered industrial lasers. As in other surface transformation hardening processes, the object of laser surface hardening is to generate a relatively thin surface layer in which the material has undergone martensitic transformation. The process is, therefore, limited to materials that are capable of undergoing such a transformation; or in other words, to hardenable cast irons and steels.

In order for such materials to harden by martensitic transformation, they must be heated to a temperature at which the austenitic phase is stable, followed by very rapid cooling, or quenching, to room temperature.

In surface hardening only the surface region of the workpiece needs to be heated to austenitizing temperatures. It is desirable that this surface heating takes place as rapidly as possible, in order to minimize the effect of heating on the bulk of the material. This requires a very high heat flux to be applied to the workpiece surface. In essence, heat must be applied to the surface at a higher rate than it can be conducted away from the surface towards the cold interior. This makes the laser an ideal heat source for surface hardening of cast irons and steels. In fact, the laser is capable of heating the surface so rapidly that the required subsequent quenching occurs by heat conduction to the still cold interior of the workpiece.

This process, known as self-quenching, is one of the great advantages of laser surface hardening.

When the laser is used for surface transformation hardening, the required power density (flux) is lower and the exposure time longer than in processes such as welding or cutting.

A convenient way of achieving this is to reshape the laser output beam to a broad area beam with uniform power density rather than to the focused beam used for welding and cutting. A typical broad area laser beam, suitable for surface transformation hardening, may have the shape of a square with dimensions of the order 1 cm x 1 cm in the focal plane, and have a power density of 5×10^2 to 5×10^3 w/cm^2. Hardening is performed by moving such a spot over the workpiece surface at controlled speed. If the processing parameters (power and speed) are appropriate, a strip of surface hardened material is generated by the moving laser spot, and the depth of this hardened case can be controlled through the control of these parameters.

The laser output beam can also be shaped into other suitable broad area beams by means of various optical devices, depending on the specific applications. However, in this program, a square spot with dimensions 1.27 cm x 1.27 cm (0.5" x 0.5") was used throughout.

The absorption of laser radiation from a CO_2 laser (10.6μm) in metals is very low at room temperature. With the relatively low power densities used in surface hardening, it is, therefore, necessary to use energy absorption coatings on the workpiece surface. Many different substances have been used for this purpose, such as manganese phosphate and paints containing graphite,

silicon and carbon black. Since many of the coatings that have been used are quite effective, the choice of a particular coating is dictated not so much by its relative absorption efficiency, as by other considerations such as ease of application and post-processing removal of coating residue. In the work reported here, flat black Krylon #1602 spray paint was used. This coating appears to be 80-90% effective in overall absorption of the 10.6 μm laser radiation. It is easy to apply and is not very sensitive to variation in coating thickness, as long as care is taken to ensure complete coverage. The residue left by this coating after laser processing is also easy to remove.

2.1.2 Metallurgy

In conventional hardening of steel, the workpiece is brought up to austenitizing temperatures at a relatively slow rate, and then allowed to soak at this temperature before quenching. This allows sufficient time for homogenous austenite to form throughout the workpiece, which upon quenching will be transformed to martensite.

In laser surface transformation hardening, the situation is somewhat different because the heating time is very short and no isothermal soak takes place in this process. The very rapid heating and the short time that the workpiece material is kept at elevated temperatures result in several metallurgical effects which must be taken into consideration in analyzing the process.

First of all, rapid heating leads to an increase in the observed transformation temperature[1)], which can result in a thinner hardened case than otherwise would

be expected. This effect will, of course, become more pronounced as the laser processing speed increases and the exposure time decreases.

Secondly, if the structure of the workpiece is such that the carbon is unevenly distributed in the micro-structure, the short time the material is at temperatures above the transformation temperature is not sufficient to allow the carbon to redistribute itself uniformly in the austenitic phase. The resulting austenite will, therefore, be of variable carbon content and the structure obtained after self-quenching will not be uniform[2]. This is not a problem with reasonably fine-grained, medium and high carbon steels, but if the material contains appreciable amounts of free ferrite, such as low carbon steel or some nodular cast irons, laser surface hardening may not be possible in practice. This is particularly so if the material is relatively coarse-grained. Such materials can, however, be laser hardened if they are given a pre-processing quench and temper heat treatment. If the tempering temperature is not too high such a material will have its carbon in a finely dispersed form, and can be laser surface hardened.

Because the laser hardening process takes place under conditions of unsteady heat flow, it is necessary to heat the workpiece surface to temperatures considerably above the normal austenitizing range, in order to obtain useful heat penetration and case depth. The surface will, therefore, experience much higher temperatures than in conventional hardening practices. Care must be taken to prevent the surface temperature from reaching the melting point, particularly in cases where a very deep case is to be generated.

In some cases, localized grain growth may occur if the surface temperature approaches the melting point. Because the maximum temperatures will often occur in the neighborhood of corners and fillets, such grain growth may be very detrimental.

There is also some indication that areas that have been brought to a very high temperature may show excessive amounts of retained austenite after quenching.

The depth of hardened case that can be obtained in laser surface transformation hardening also depends on the hardenability of the material and on the size of the workpiece. A large workpiece, made from a material with good hardenability, can be processed at low speed because a high rate of self-quenching is not required. Hence, there is sufficient time available for deep heat penetration and a deep case can be generated. In SAE 4340 steel, for example, case depths in excess of 0.1" are easy to obtain.

In materials with low hardenability, such as low carbon steel, the laser processing speed must be higher in order to obtain high self-quenching rates. This is particularly true if the workpiece is small and thus is a limited heatsink. A steep temperature gradient must be generated in the workpiece, but because the maximum surface temperature is limited by the melting point of the material, only limited hardened case can be obtained in such materials.

2.1.3 Heat Flow in Laser Surface Transformation Hardening

In order to predict the results of laser surface transformation hardening with a broad area beam, it is necessary to evaluate the time dependent tempera-

ture distribution in the workpiece in the vicinity of of the moving laser spot. Because the boundary conditions are favorable, it is possible to obtain closed solutions to the generalized heat flow equation

$$\alpha \nabla^2 T = \frac{\partial T}{\partial t} \qquad 1)$$

that are useful for such prediction. If we consider the semi-infinite body, Equation 1) reduces to

$$\frac{\partial Q}{\partial t} = \alpha \frac{\partial^2 Q}{\partial Z^2} \qquad 2)$$

where α is the thermal diffusivity; Z, the depth below the surface; $Q = -K\ {}^{\partial T}/_{\partial Z}$ is the flux and K is the thermal conductivity. If the flux at the surface is constant, the boundary conditions are:

The solution to Equation 2) is then[3)]

$$\nabla T = \frac{2Q_i \xi}{K} \sqrt{\alpha t}\ i\,erfc\ \frac{Z}{Z\sqrt{\alpha t}} \qquad - \qquad 3)$$

where ΔT at the temperature rise; Q_i is the applied flux, ierfc stands for the integrated error function compliment and ξ is the emmisivity of the material, specific to temperature and wavelength of the laser radiation.

This solution is only valid for a semi-infinite body with uniform flux at the surface; i.e., when there is no lateral heat flow so that the heat flow is uni-directional.

This condition is, however, approximately true for the centerline of a broad area laser spot with uniform power distribution, provided the spot is large compared to the characteristic heat diffusion distance

$$d = (\alpha t)^{1/2} \qquad 4)$$

where t_D is the dwelltime (exposure time). For a square spot with dimensions bxb, this time is:

$$t_D = b/v \qquad 5)$$

where v is the velocity of the laser spot. Hence, if

$$\frac{b}{2} \gg (\alpha t_0)^{1/2} \qquad 6)$$

Equation 3) will correctly give the temperature at the centerline of the laser spot. In practice, it is found that if $b \geq 16d/v$, good agreement with experimental data can be obtained. We can then rewrite Equation 3) in the form

$$T_T = T_0 + \frac{2Q_i\varepsilon}{k}\sqrt{\alpha t_D}\, i\,\mathrm{erfc}\,\frac{\delta_H}{2\sqrt{\alpha t_D}} \qquad 7)$$

where T_T is the transformation temperature, T_o is the room temperature, and δH is the depth of case.

This equation can also be used to estimate the cooling rate resulting from the self-quenching effect behind the moving laser spot. By the superposition principle, the temperature on the centerline behind the laser spot is approximately:

$$T = T_o + \frac{2Q_i\varepsilon}{K}\left[\sqrt{\alpha t}\, i\,\mathrm{erfc}\,\frac{z}{2\sqrt{\alpha t}} - \sqrt{\alpha(t-t_o}\, i\,\mathrm{erfc}\,\frac{z}{2\sqrt{\alpha(t-t_o}}\right] \quad 8)$$

where t is the total elapsed time from the start of heating and $(t-t_D)$ is the cooling time. Because of the requirements for minimal lateral heat flow discussed above, this equation can only be used for high speed processing and small values of the cooling time $(t-t_D)$.

If the processing speed is so low that Equation 7) cannot be used; that is, if the heat flow is three-dimensional in the vicinity of the centerline of the laser spot, a more involved analysis is required. An expression, valid for the semi-infinite body with three-dimensional flow around a rectangular spot, is given by Carslaw and Jaeger [4]. A modification, derived on slightly different principles and valid for a plate with finite thickness was developed in conjunction with this program. The temperature distribution around the moving laser spot under these conditions, was found to be [5]

$$T = T_o + \frac{Q_i\varepsilon\alpha}{2K\nu\sqrt{\pi}}\int_0^{\prime\prime}\sum_{m=-\infty}^{m=\infty}\exp-\left[\frac{(2mD-Z)\omega}{1-\omega}\right]^2\cdot\left[\mathrm{erf}\,\frac{(Y+L)\omega}{1-\omega} - \mathrm{erf}\,\frac{(Y-L)\omega}{1-\omega}\right]\cdot\left[\mathrm{erf}\,\frac{2(X+B)\omega^2-(1-\omega)^2}{2\omega(1-\omega)} - \mathrm{erf}\,\frac{2(X-B)\omega^2-(1-\omega)^2}{2\omega(1-\omega)}\right]\frac{d\omega}{\omega^2} \quad 9)$$

where erf stands for the error function and:

$$X = \frac{vx}{2\alpha} \qquad B = \frac{vb}{4\alpha}$$

$$Y = \frac{vy}{2\alpha} \qquad L = \frac{v\ell}{4\alpha}$$

$$Z = \frac{vz}{2\alpha} \qquad D = \frac{vd}{2\alpha}$$

b = length of laser spot.
ℓ = width of laser spot.
d = thickness of plate.

In using these models for the prediction of hardened case, it is necessary to know the intensity of the actually absorbed flux, the average value of the thermophysical constants K and α (thermal conductivity and thermal diffusivity) in the temperature range experienced by the workpiece during processing, and the temperature at which the material will transform to austenite.

The fraction of the applied power that is absorbed into the workpiece (the emissivity ξ), depends among other things on the condition of the workpiece surface. For clean metal surfaces, the emissivity at the wavelength of the CO_2-laser (10.6 μm) is very low. However, by using various absorbing coatings, the emissivity can be increased to the 0.8-0.9 range, even at the relatively low power densities used in surface hardening. In this work, flat black Krylon #1602 spray paint was used as an energy absorber. This increased the absorption to an estimated value of 85%.

The values of the thermal conductivity, K, and the thermal diffusivity, α, for hardenable ferrous materials, changes fairly rapidly with the temperature. Hence, the room temperature values of these variables cannot be used for case depth prediction.

However, in cases where the variation of K and α with the temperature are known, the integral average value can be calculated as:

$$\bar{K} = \frac{1}{T_2 - T_1} \int_{T_1}^{T_2} K(T)\, dT \qquad 10)$$

$$\bar{\alpha} = \frac{1}{T_2 - T_1} \int_{T_1}^{T_2} \alpha(T)\, dT \qquad 11)$$

by means of numerical integration.

In this work, case prediction was performed partially by the aid of Equation 9) and 10), partially by experimental determination of K and α from preliminary runs, as described in Section 2.2.5.

The final datum needed for case prediction is the transformation temperature. This is, of course, not a fixed temperature unless the steel has eutectoid composition. Furthermore, the temperature range over which the transformation occurs is sensitive to the processing speed. In this work, we have used the A_f temperatures from the pertinent IT diagrams as the transition temperature T_T.

2.2 Experimental Work

2.2.1 Equipment and Procedures

The experimental surface transformation hardening was performed with an Avco HPL®-10 CO_2 laser. This laser was capable of up to 15 kW output (CW).

The collimated output beam from the laser was directed through ducts to the workstation. In the workstation, the beam - approximately 2.6" in diameter - was shaped to a convergent, square beam by means of an optical integrator, as shown in Figure 1. The square beam had dimensions 1/2" x 1/2" in the focal plane.

Surface transformation hardening was performed on plane specimens by moving the specimens under the beam at controlled speed. The specimens were mounted on a milling machine table in such a way that the focal plane of the optical integrator was located on the specimen surface. The translation speed of the table could be varied steplessly, and speed calibration curves were established prior to start of processing. The correct location of the specimen relative to the beam could be determined by means of a low powered He-Ne laser locator beam built into the laser system to give a visual representation of the location of the actual power beam prior to processing.

The laser power could also be varied steplessly, from approximately 1 kW up to full power. The actual power delivered to the workpiece was determined by calibration curves, established in advance by means of calorimetric measurements. In addition, the beam quality (sharp edges and even power density) was assessed by making test burns in lucite blocks. Speed and power calibration, as well as beam quality, was checked periodically during processing of the samples. Figure 2 shows schema-

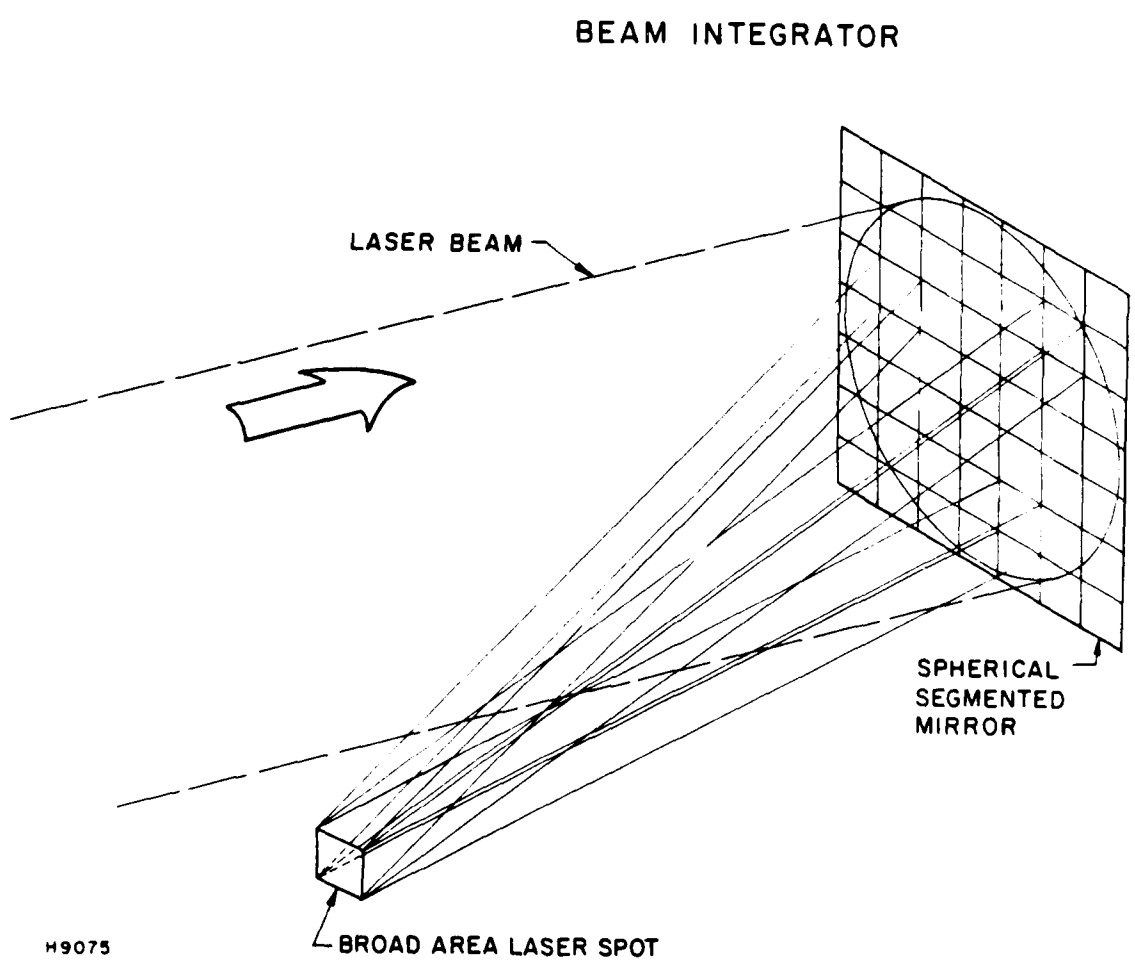

FIGURE 1 FORMING A BROAD AREA LASER SPOT BY MEANS OF AN OPTICAL INTEGRATOR

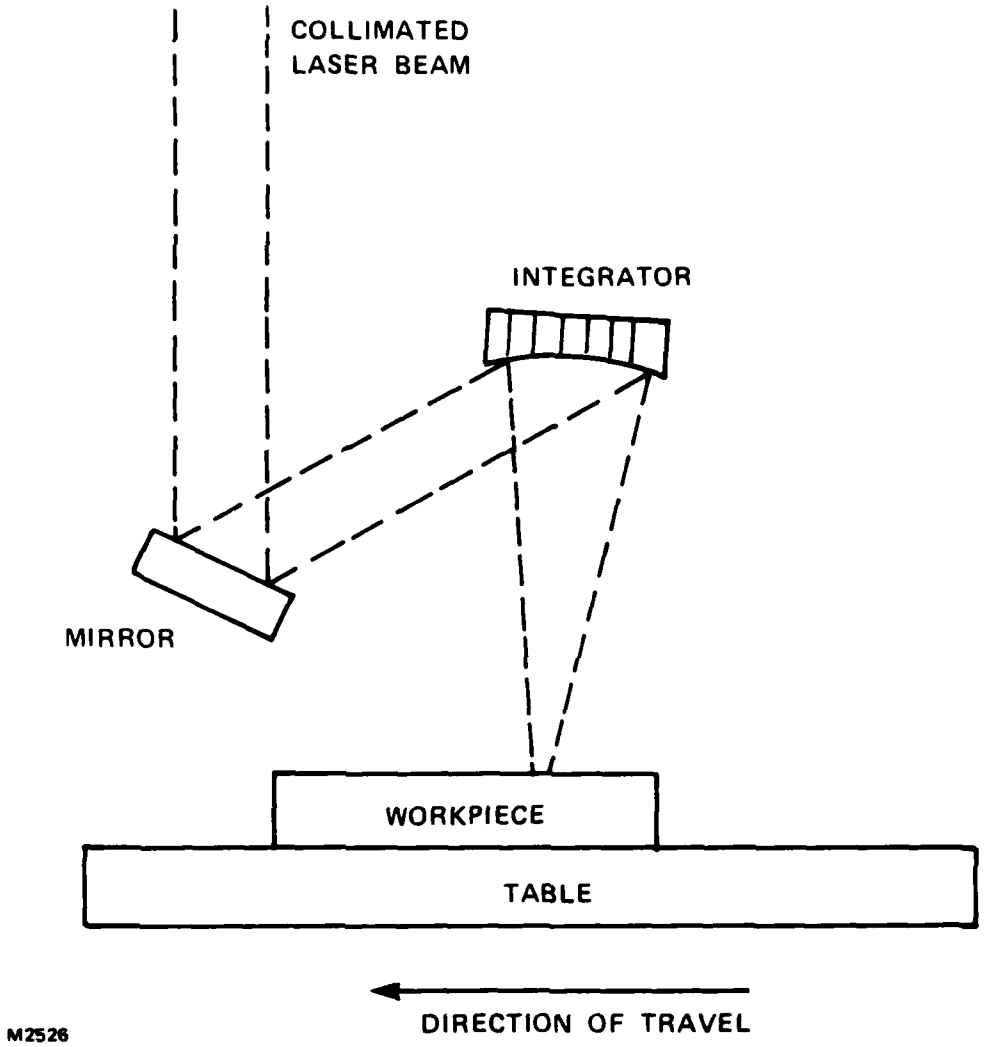

FIGURE 2 SETUP FOR LASER TRANSFORMATION HARDENING OF FLAT PLATES

tically the experimental setup used for this program.

Prior to processing, the workpiece surfaces were prepared by coating with flat black Krylon #1602 spray paint. This was done in order to enhance the absorption of the laser radiation (10.6 μm) into the workpiece surface. Previous experience has shown that this treatment results in approximately 85% absorption of the CO_2 laser radiation, even at relatively low power densities. Furthermore, this type of coating is easy to put on, leaves little residue for post-processing cleanup, and is not very sensitive to small variation in application technique. No protective atmosphere was used during processing, but a fan blowing crosswise over the beam/workpiece interaction zone was used to dissipate the smoke resulting from pypolysis of the coating.

The results of the laser processing were evaluated by metallography and micro-hardness testing, using a Knoop Indenter with 500g load.

2.2.2. Case Prediction by One-Dimensional Heat Flow Model

Prior to the experimental laser processing, the processing parameters were estimated, using a calculator code built on one-dimensional heat flow considerations, as discussed in Section 2.1.2.

The program was written for use on a Texas Instrument TI 59 programmable calculator/printer. This program predicted maximum surface temperature and depth of case based on processing parameters (speed and power density), thermophysical constants and transition temperature of the material.

Originally, this program did not contain any cut-off for processing parameters that fell outside the range where the one-dimensional heat flow model was valid. The

predicted case depth did not, therefore, show reasonable agreement with experimentally obtained data for low processing speed. The program was, subsequently, rewritten to reject input data of this kind. The program could also be used to predict cooling rates during self-quench, based on Equation 8), Section 2.1.3.

The flow sheet of the program is shown in Figure 3, and the complete program with user information is listed in Appendix I.

The thermophysical constants used in the preliminary phase were calculated from published data [6], as described in Section 2.1.3. The constants for the materials surveyed in the preliminary phase are given in Table I.

2.2.3. Preliminary Evaluation of Laser Hardening Parameters

In this preliminary evaluation phase, the response of six different materials to laser surface hardening was surveyed. The materials were SAE 1045 in the quenched and tempered condition (Q/T), SAE 1045 in the hot-rolled condition (H.R.), SAE 4140 in the Q/T and H.R. condition, SAE 1020 in the H.R. condition and SAE 4340 in the cold-rolled condition (C.R.). Samples of these materials were supplied by FMC/NOD in the form of plates with minimum dimensions 1/2" thick by 2" wide by 8" long.

These specimens were laser processed as described earlier, making single, well separated straight laser runs on the surfaces of the specimens. The processing parameters (power and speed) were varied within limits, calculated to give case depths in the range 10 to 120 mil (0.025 to 0.305 cm). The predicted case was calculated in advance in each case, using the calculator program described in Section 2.2.2.

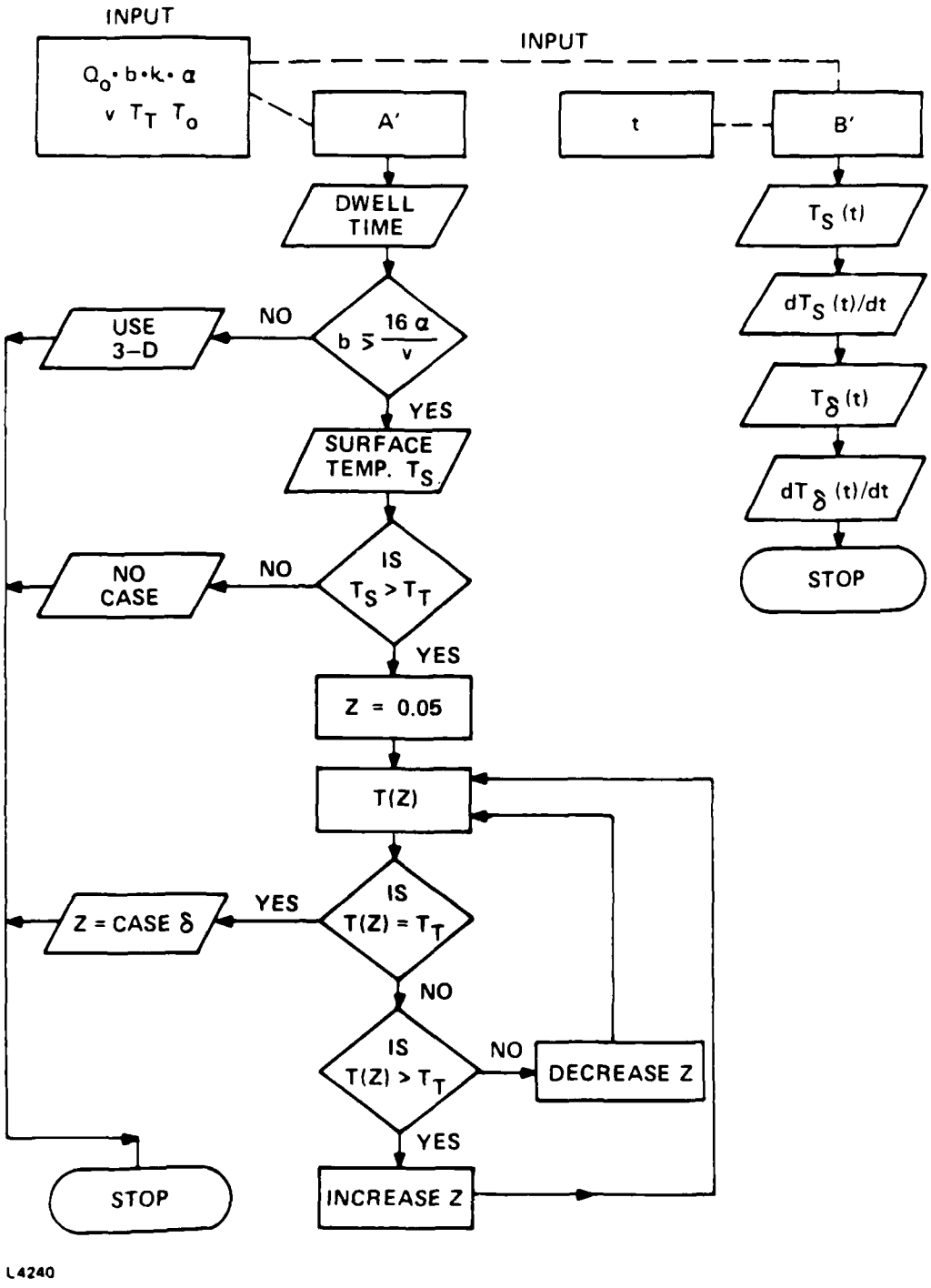

FIGURE 3 PROGRAM FOR PREDICTION OF CASE DEPTH AND COOLING RATE

TABLE I

THERMOPHYSICAL CONSTANTS (Estimated) FOR VARIOUS STEELS

Material	Thermal Cond. K (w/cm-C°)	Thermal Diff. α (cm^2/sec)	Transition Temp. T_T C°
SAE 1020	0.38	0.087	850
SAE 1045	0.36	0.085	790
SAE 4140	0.33	0.072	780
SAE 4340	0.30	0.063	750

The processed specimens were analyzed at FMC/NOD for case depth and surface hardness. The results are given in a preliminary report[7] from FMC/NOD, and are summarized in Tables II, III, IV and V. Due to the limits set by the total available laser power, large areas cannot be laser hardened without some form of multiple-pass technique. It is, however, of interest to look at the best way of achieving this. Several straight abutting and overlapping laser runs were made on samples of SAE 4140 (Q/T), and the discontinuity of hardened case in the zones between the runs assessed by surface hardness measurements. The results are shown in Figures 4, 5 and 6.

2.2.4 Discussion of Preliminary Results

The results of the preliminary processing, as given in Tables II through V, show good agreement between predicted and measured case for medium processing speed. The correlation is, however, poor for very high speed (60 in/min, 2.54 cm/sec) and for very low speed (5-10 in/min, 0.21-0.42 cm/sec). For the high speed runs the casedepth is much higher than predicted; while for low speed, the reverse is the case. The latter observation can be attributed to the fact that the one-dimensional heat flow model used is not valid at these low speeds. Hence, the actual temperatures reached by the workpiece surface are much less than those predicted, due to lateral heat flow in the workpiece.

The underestimation of case depth for the high speed runs is unexpected and difficult to explain. If anything, a shallower depth than predicted would not be surprising in this case because the heating rate is so rapid that the kinetics of the process could be expected to influence the results. Lacking any rational explanation for this phenomenon, it is, therefore, assumed that some

115% OF THEORETICAL
STANDARD DEVIATION
59.6%

SAE 4140

$\alpha = 0.072\ cm^2/sec$

$T_T = 780°\ C$

CONDITION	POWER (kW)	SPEED (in/min)	CALCULATED CASE (mil)	MEASURED CASE (mil)	% OF THEORETICAL	CALCULATED SURFACE TEMP. (C°)	SURFACE HARDNESS (Rc)
Q/T	2.5	30	49	47	96	1203	57
Q/T	2.5	40	29	37	128	1045	56.5
Q/T	2.5	60	8	18	225	856	57.5
Q/T	2.0	15	88	77	88	1369	55.5
Q/T	1.7	15	66	63	95	1174	56.5
Q/T	1.5	15	48	45	94	1045	55.5
Q/T	1.4	10	95	56	59	1275	56.5
H.R.	2.5	30	49	48	98	1203	43.5
H.R.	2.5	40	29	40	138	1045	45.0
H.R.	2.5	60	8	22	275	856	27.0
H.R.	2.0	15	88	71	81	1369	37.0
H.R.	1.7	15	66	54	82	1174	31.5
H.R.	1.5	15	48	45	94	1045	31.5
H.R.	1.4	10	95	53	57	1275	37.5

144% OF THEORETICAL
STANDARD DEVIATION
90.1%

SAE 1045

$\alpha = 0.085\ cm^2/sec$

$T_T = 790°\ C$

CONDITION	POWER (kW)	SPEED (in/min)	CALCULATED CASE (mil)	MEASURED CASE (mil)	% OF THEORETICAL	CALCULATED SURFACE TEMP. (C°)	SURFACE HARDNESS (Rc)
Q/T	2.5	30	51	50	98	1198	55
Q/T	2.5	40	30	38	127	1040	57
Q/T	2.5	60	7	24	342	853	55.5
Q/T	2.5	28	57	67	118	1239	55.5
Q/T	2.3	60	NIL	16	-	769	55.5
Q/T	2.1	40	13	20	154	882	55.5
Q/T	3.0	40	51	51	100	1278	54
H.R.	2.5	30	51	46	90	1198	47.5
H.R.	2.5	40	30	34	113	1040	50
H.R.	2.5	60	7	24	342	853	44
H.R.	3.0	40	51	51	100	1278	50

83% OF THEORETICAL
STANDARD DEVIATION
8.3%

SAE 1020

$\alpha = 0.087\ cm^2/sec$

$T_T = 850°\ C$

CONDITION	POWER (kW)	SPEED (in/min)	CALCULATED CASE (mil)	MEASURED CASE (mil)	% OF THEORETICAL	CALCULATED SURFACE TEMP. (C°)	SURFACE HARDNESS (Rc)
C.R.	1.9	30	6	NIL	-	887	31
C.R.	2.1	30	18	17	94	975	40
C.R.	2.3	30	29	25	86	1062	43
C.R.	2.45	30	38	27	71	1150	46
C.R.	2.6	30	47	38	81	1273	46.5

86.7% OF THEORETICAL
STANDARD DEVIATION
24.3%

SAE 4340

α = 0.063 cm^2/sec

T_T = 750° C

CONDITION	POWER (kW)	SPEED (in/min)	CALCULATED CASE (mil)	MEASURED CASE (mil)	% OF THEORETICAL	CALCULATED SURFACE TEMP. (C°)	SURFACE HARDNESS (Rc)
C.R.	2.4	30	49	45	92	1190	49.5
C.R.	2.3	40	27	26	96	992	51
C.R.	2.3	60	7	10	143	814	48.5
C.R.	1.6	10	110	75	68	1393	53
C.R.	1.6	15	63	54	86	1141	53
C.R.	1.4	15	45	40	89	1007	48.5
C.R.	1.9	15	85	73	86	1341	55
C.R.	1.3	10	78	55	71	1148	48
C.R.	1.0	5	116	57	49	1175	52.5

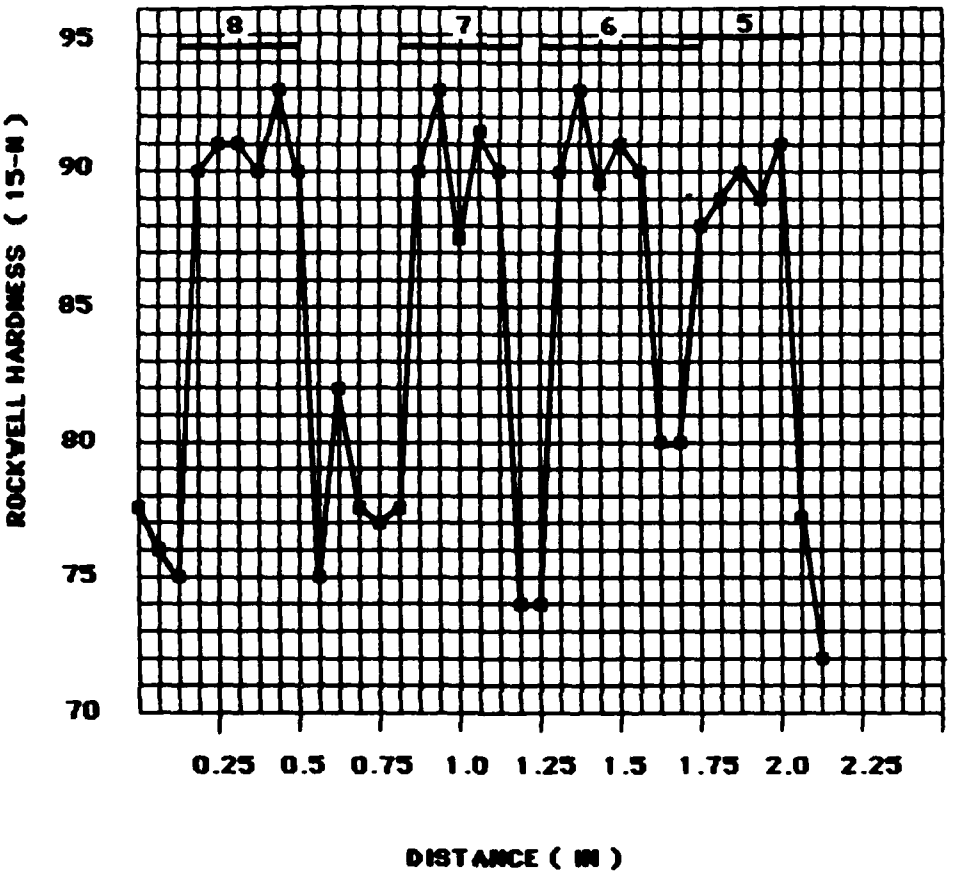

FIGURE 4.

SURFACE HARDNESS OF OVERLAPPING RUNS ON
SAE 4140 STEEL (H.T.)
POWER DENSITY 1290 W/cm^2
PROCESSING SPEED 40 IN/MIN
RUNS 5-8

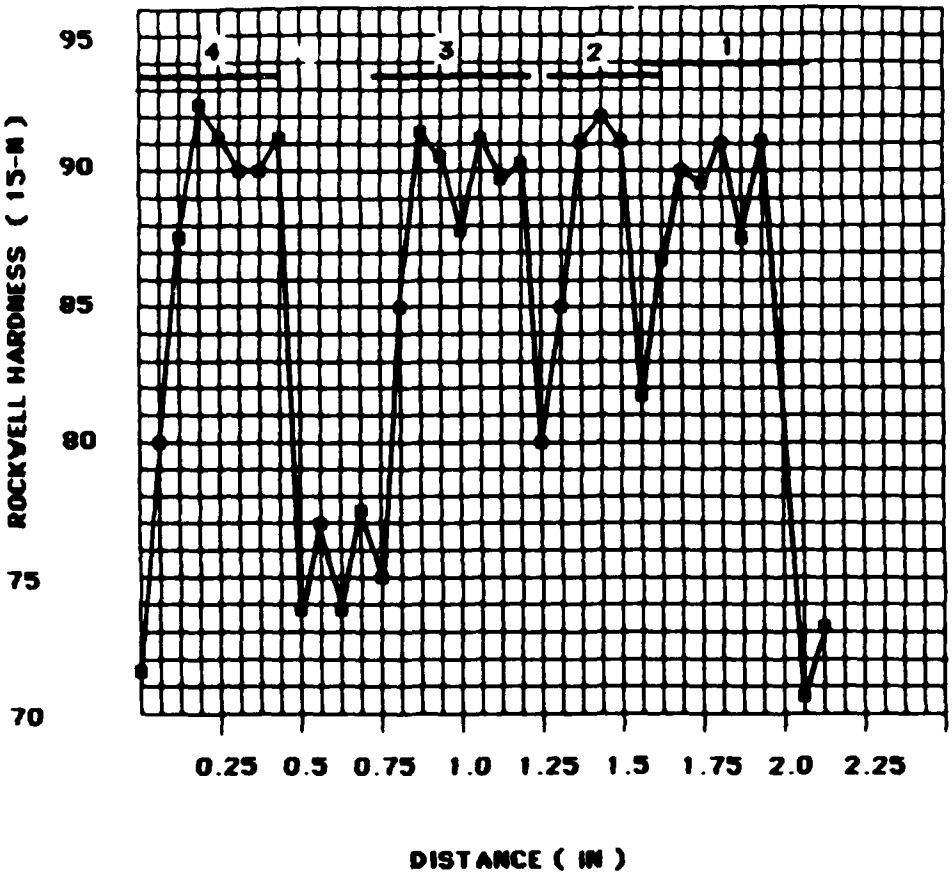

FIGURE 5

SURFACE HARDNESS OF OVERLAPPING RUNS ON
SAE 4140 STEEL.
POWER DENSITY 1290 w/cm^2
PROCESSING SPEED 30 IN/MIN.
RUNS 1-4.

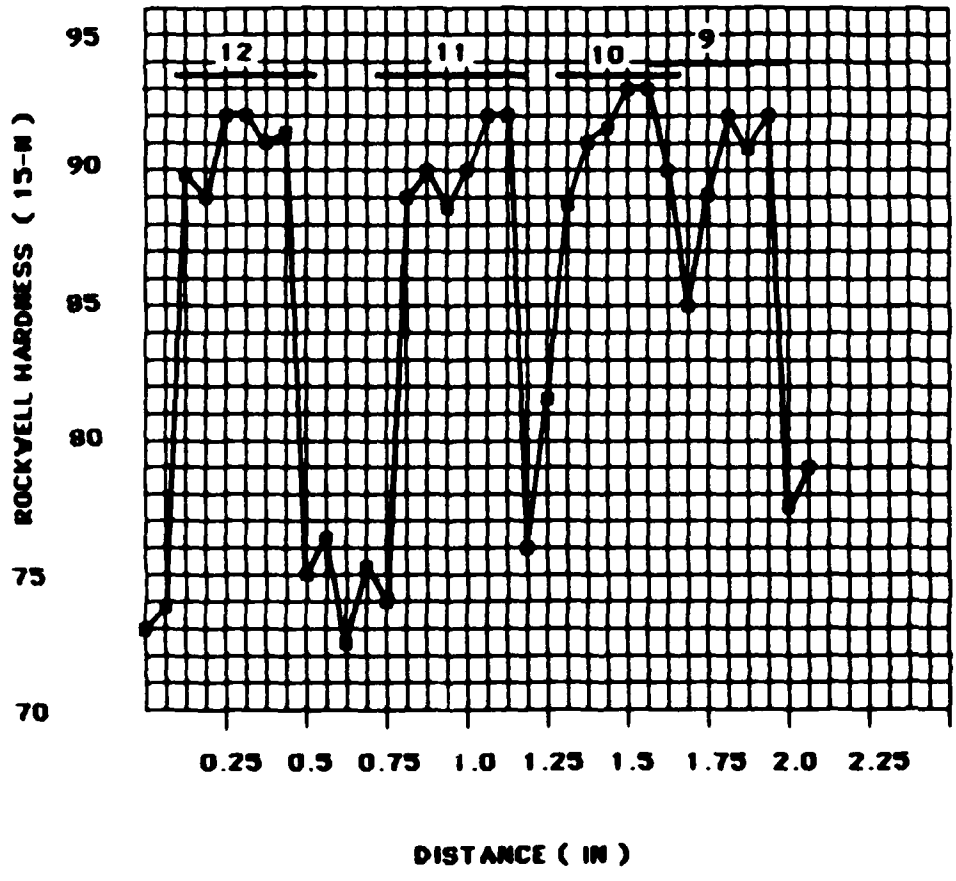

FIGURE 6.

SURFACE HARDNESS OF OVERLAPPING RUNS ON
SAE 4140 STEEL.(H.T.)
POWER DENSITY 790 W/cm^2
PROCESSING SPEED 15 IN/MIN.
RUNS 9-12

error was made in the power setting, or more possible in the speed calibration curve, in such a way that the actual translation speed was lower than the assumed speed.

For most of the materials, the limit of effective case was taken to be the depth at which the hardness had decreased to Rockwell C 45. In SAE 1020, this criterion could not be used, since the maximal hardness at 100% martensite is about equal to this. Hence, in this case, Rockwell C 35 was used as limit of effective case.

Several of the materials, in particular SAE 4140 (H.R.) and SAE 1045 (H.R.), showed very low surface hardness. This was due to some surface decarburization in these materials. Both materials showed full hardness at greater depth below the surface.

These preliminary studies show the need for the following improvements in the procedures used for the materials response survey:

- elimination of decarburized surface layers in the test specimens,
- improved model for case prediction, including better data for the thermophysical constants,
- closer control of processing parameters, particularly processing speed.

The results of the overlap runs, given in Figures 4,5 and 6, show that uniform hardened case across the specimen surface cannot be obtained with parallel, multiple laser runs. If the runs are overlapping, some backtempering will occur in the overlap zone. The minimum hardness in this zone is, however, well above the

bulk hardness. Hence from the criterion of surface hardness alone, overlapping runs appear to be more effective than abutting or adjacent runs.

2.2.5 Improved Model for Prediction of Case Depth

As explained in Section 2.1.2., it is possible to obtain a closed solution to the heat flow equation, even if the conditions for one-dimensional heat flow are not met. The solution to the three-dimensional heat flow around a rectangular laser spot on the surface of a finite plate, Equation 9), is, however, very complex and time-consuming to use for practical purposes. It can be simplified somewhat by assuming the workpiece to be infinitely thick. (This is a valid assumption for the range of processing parameters used in this work, provided the actual plate thickness is not less than 1/4"). Furthermore, since a square spot is used in this work and we can limit our calculations to points on or below the centerline of the laser spot, we can rewrite Equation 9) in the form:

$$T = T_0 + \frac{2Q_i \varepsilon \alpha}{2K_1 \pi \sqrt{\pi}} \int_0^1 \exp - \left[\frac{z\omega}{1-\omega}\right]^2 \cdot \left[\operatorname{erf} \frac{L\omega}{1-\omega}\right] \cdot \qquad (12)$$

$$\left[\operatorname{erf} \frac{2(x+B)\omega^2 + (1-\omega)^2}{2\omega(1-\omega)} - \operatorname{erf} \frac{2(x+B)\omega^2 + (1-\omega)^2}{2\omega(1-\omega)}\right] \frac{\omega\, d\omega}{\omega^2}$$

This is still a formidable expression to evaluate because the numerical integration requires some 50 to 100 ordinate evaluations in order to give sufficient accuracy. Furthermore, we are interested in finding the maximum value of the temperature relative to the laser spot, and

we have no a priori knowledge where this maximum occurs. To make the model more readily useful, the following procedure was adopted. First, the temperature maximum on or directly below the centerline was evaluated for various paired values of the parameters B and Z in the speed region where three-dimensional heat flow dominates.

Secondly, by comparing these results to those obtained through the use of the one-dimensional heat flow equation (Equation 2), it was found that the ratio f between these two values

$$f = \frac{T(3\text{-}D)}{T(1\text{-}D)} \qquad 13)$$

could be expressed with good accuracy as a polynomial in the form:

$$f = (a_1 B^2 + b_1 B + C_1)\left(Z/B\right)^2 + (a_2 B^2 + b_2 B + C_2)\cdot\left(Z/B\right) + (a_3 B^{-2} + b_3 B^{-1} + C_3) \qquad 14)$$

provided the range of B values in each case was not too large. By dividing the range of B values between 0.5 and 4 into three intervals, the constants in Equation 14) could be found by regression analysis.

For values of $B \geq 4$, f is unity; i.e., the one-dimensional heat flow model is valid. A calculator program, incorporating Equation 14), could then be written in such a way that case depth values could be predicted for the entire range of processing parameters used in this work. The flow sheet of the program is shown in Figure 7, and the complete program with used instructions is listed in Appendix II.

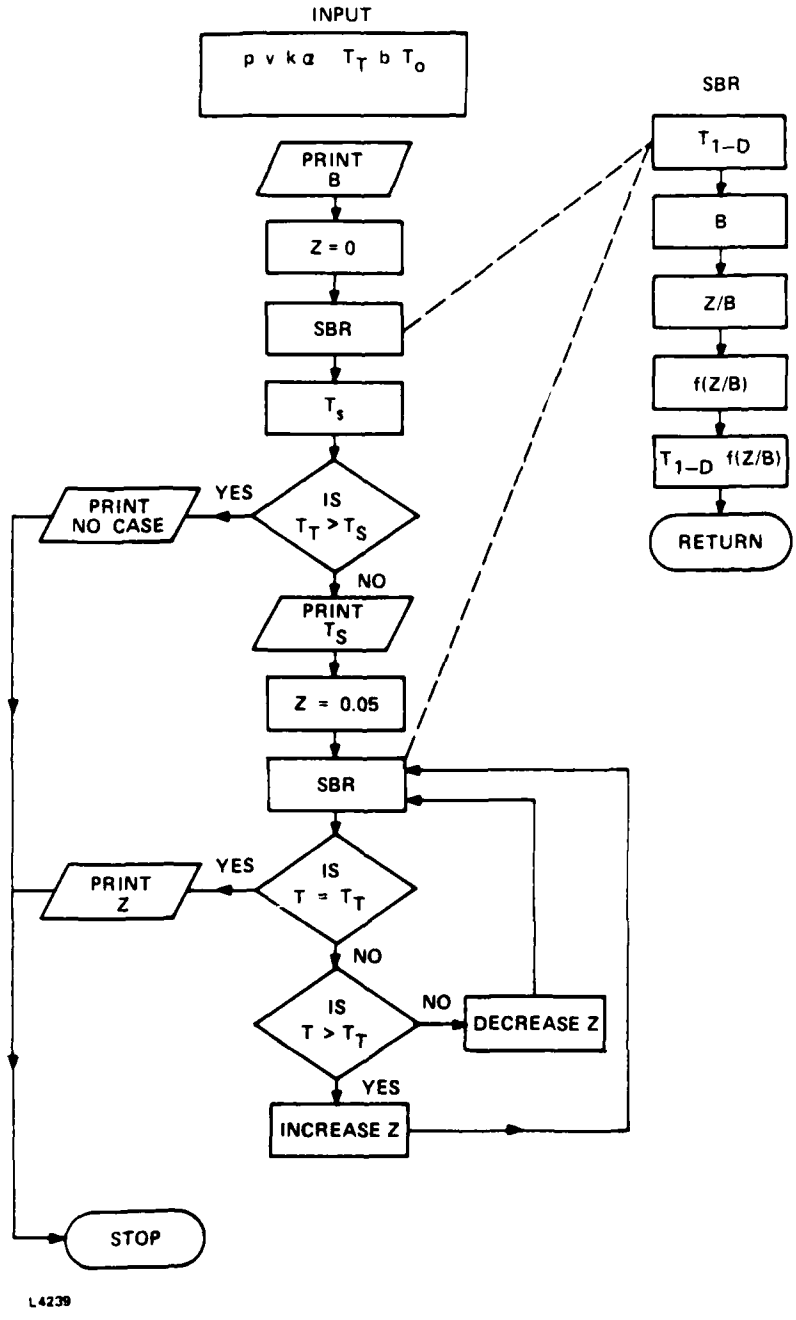

FIGURE 7 IMPROVED PROGRAM FOR CASE DEPTH PREDICTION

2.2.6. Experimental Evaluation of the Thermophysical Constants

As discussed in Section 2.1.2., the thermophysical constants K and α can be estimated for the purpose of case depth prediction, by calculating the integral average of these constants over the approximate temperature range of processing. Unfortunately, however, adequate data for the variation of K and α with the temperature is only available for a few steels. This is particularly true for the diffusivity α. To obtain more general and realistic values for K and α, the following procedure was adopted for the final phase of this work.

1) The thermal conductivity K was determined as before by calculating the integral average over the temperature range of processing, using published data and Equation 10). For materials where only the room temperature conductivity was available, the average value of K was estimated from this datum, relative to materials for which complete data was known.

2) A number of trial laser runs were made, using processing speeds sufficiently high to ensure predominantly one-dimensional heat flow. The resulting case depths were measured by means of micro-hardness testing, and the value of the diffusivity α for each material was then found by least mean square analysis, using the experimentally determined case depths and the value of conductivity K, (found from step 1) in Equation 7). Due to the transcendental nature of this equation, the analysis had to be done by numerical methods. This method of determining the average thermal

diffusivity is phenomenological and is not intended to represent anything else but an empirical parameter for practical work. The method has the advantage of expressing the value of α based on actual processing, and an error in the estimation of K will, at least in part, be compensated for due to the fact that the results obtained through Equation 7) are more dependent on the ratio of K and α then on their individual values. The values of K and α used in the final part of this work are given in Table VI. Some of the values for K, given in Table I, have been recalculated over a larger temperature interval and are, therefore, somewhat smaller. Here, it is noticeable that the new values of α, found by experimental methods, are significantly lower than the earlier values found by integral averaging.

2.2.7. Final Evaluation of Processing Parameters

In this final phase, steels in various heat treated conditions were laser processed over a wide range of processing parameters. The sample materials consisted of SAE 1045 in the annealed (ANN.) condition, the quenched and tempered (Q/T) condition and in the hot-rolled (H.R.) condition, SAE 4140 in the ANN., Q/T and H.R. condition, SAE 4340 in the ANN., Q/T and H.R. condition, SAE 8620 in the ANN. and Q/T condition, and Hyten B 3X in the ANN. and Q/T condition. Samples of SAE 1020 and SAE 4130 were also supplied by FMC/NOD, but these materials were not suited for parameter development work, as explained in Section 2.2.8 below. The samples consisted of plates and bars, none with thickness less than 1/2". All samples were processed in the same manner described in Section 2.2.1. In each case, the expected case depth was

TABLE VI

THERMOPHYSICAL CONSTANTS

MATERIAL	THERMAL COND. K (w/cm - c°)	THERMAL DIFF. α (cm^2/sec)	TRANSITION TEMP. Tr (c°)
SAE 1045	0.36	0.068	790
SAE 4140	0.31	0.049	780
SAE 4340	0.28	0.047	750
SAE 8620	0.28	0.050	840
HYTEN B3X	0.30 (est.)	0.049	760 (est.)

predicted in advance, using the improved calculator program discussed in Section 2.2.5 above. The results of the processing are given in Tables VII through XI.

In addition, adjacent and overlapping runs in the pattern shown in Figure 8, were made on samples of SAE 8620 and Hyten B 3X. The results of these runs are shown in Figures 9 through 16. The hardness profiles shown in these figures were not obtained by surface hardness measurements, but by micro-hardness measurements taken 10 mils below the surface on samples cut normal to the processing direction.

2.2.8. Discussion of Results

The overall correlation between calculated and measured case is in the range of ±20-30% average over the entire range of processing speed and power used. The results for low speed processing of SAE 4140 and SAE 4340 are generally in even better agreement with the calculated values. This is clearly an improvement upon the results obtained in the preliminary survey.

- The values of the thermophysical constants used appear to be about right, with the exception of SAE 4340, where the value $\alpha = 0.047$ appears to be a little high.
- The surface hardness is somewhat low for most of the specimens, although full hardness is mostly achieved at ~10 mils below the surface.

  This is not uncommon in laser hardening, and it has been suggested that this is due to a lower cooling rate at the surface. However, it is easy to demonstrate that this cannot in fact be the case, as the time for cooling from A_f to M_s is shorter at the surface than in the

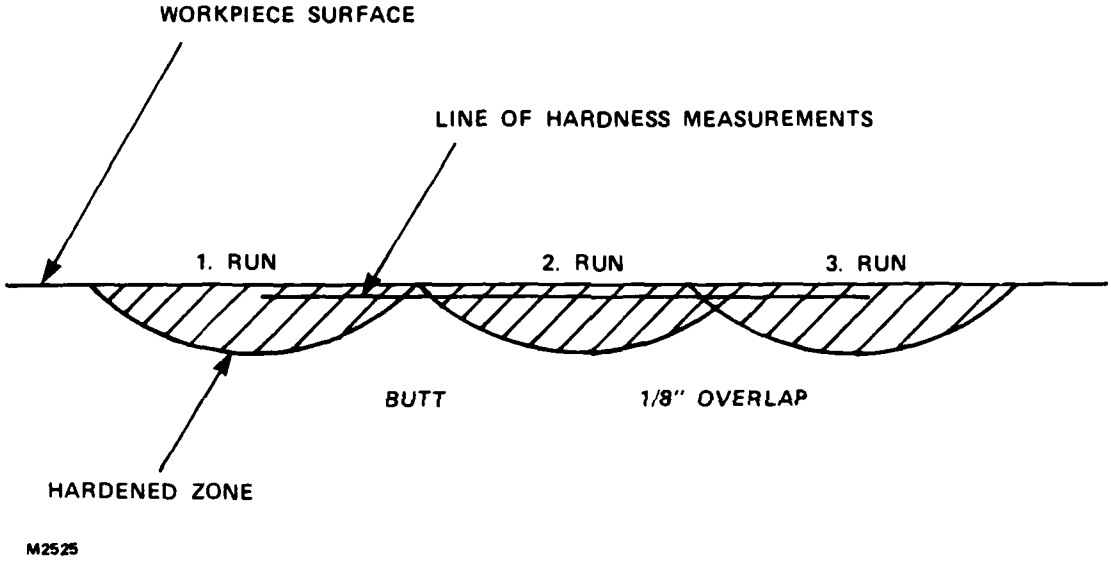

FIGURE 8 PROFILE OF OVERLAPPING RUNS

95.7% OF THEORETICAL
STANDARD DEVIATION
20%

SAE 1045

$\alpha = 0.068\ cm^2/sec$

$T_T = 790°\ C$

CONDITION	POWER (kW)	SPEED (in/min)	CALCULATED CASE (mil)	MEASURED CASE (mil)	% OF THEORETICAL	CALCULATED SURFACE TEMP. (C°)	SURFACE HARDNESS (Rc)
ANN	2.5	40	18.6	20	108	952	54.5
Q/T	2.5	40	18.6	21	113	952	56
H.R.	2.5	40	18.6	19	102	952	60
ANN	2.3	40	10.8	8	74	877	50
Q/T	2.3	40	10.8	13	120	877	52.5
H.R.	2.3	40	10.8	12	111	877	56
ANN	3.0	40	35.2	33.5	95	1139	57
Q/T	3.0	40	35.2	36	103	1139	56
H.R.	3.0	40	35.2	32	91	1139	59.5
ANN	2.5	30	36.6	24.5	67	1096	56
Q/T	2.5	30	36.6	28.5	78	1096	56
H.R.	2.5	30	36.6	31	85	1096	58
ANN	3.0	60	13.5	12.5	93	933	56
Q/T	3.0	60	13.5	13	96	933	54.5
H.R.	3.0	60	13.5	20.5	152	933	55
ANN	3.5	40	48.6	36.5	75	1325	56.5
Q/T	3.5	40	48.6	37.5	77	1325	57

100% OF THEORETICAL
STANDARD DEVIATION
28.6%

SAE 4140

$\alpha = 0.049\ cm^2/sec$

$T_T = 780°\ C$

CONDITION	POWER (kW)	SPEED (in/min)	CALCULATED CASE (mil)	MEASURED CASE (mil)	% OF THEORETICAL	CALCULATED SURFACE TEMP. (C°)	SURFACE HARDNESS (Rc)
ANN	2.3	40	8.9	12.5	140	865	52
Q/T	2.3	40	8.9	16.5	185	865	52
H.R.	2.3	40	8.9	6.0	67	865	48.5
ANN	2.3	30	23.7	16.5	70	996	57
Q/T	2.3	30	23.7	29.0	122	996	51.5
H.R.	2.3	30	23.7	16.5	70	996	52
ANN	1.4	15	13.8	17.5	127	860	53.5
Q/T	1.4	15	13.8	17.0	123	860	53.0
H.R.	1.4	15	13.8	12.5	91	860	51.5
ANN	1.6	15	31.4	22.5	72	980	52
Q/T	1.6	15	31.4	34.5	110	980	52.5
H.R.	1.6	15	31.4	22.5	72	980	52
ANN	1.7	15	39.1	32	82	1040	55.5
Q/T	1.7	15	39.1	43.5	111	1040	52
H.R.	1.7	15	39.1	34.5	88	1040	54
ANN	3.1	60	13.5	15	111	950	53.5
Q/T	3.1	60	13.5	18.5	137	950	51.5
H.R.	3.1	60	13.5	9	67	950	51.5
ANN	2.0	10	76.2	71	93	1306	53.5
Q/T	2.0	10	76.2	84.5	111	1306	52
H.R.	2.0	10	76.2	55.5	73	1306	54
ANN	1.7	5	103.7	102.5	99	1371	56.5
Q/T	1.7	5	103.7	83.5	81	1371	52.5
H.R.	1.7	5	103.7	105	101	1371	52

SAE 4340

α = 0.047 cm^2/sec

T_T = 750° C

90.2% OF THEORETICAL
STANDARD DEVIATION
23.3%

CONDITION	POWER (kW)	SPEED (in/min)	CALCULATED CASE (mil)	MEASURED CASE (mil)	% OF THEORETICAL	CALCULATED SURFACE TEMP. (C°)	SURFACE HARDNESS (Rc)
ANN	2.2	40	14.8	21.5	145	897	54
Q/T	2.2	40	14.8	13	88	897	53.5
H.R.	2.2	40	14.8	7	47	897	47.5
ANN	2.9	40	35.5	44	124	1176	55
Q/T	2.9	40	35.5	33	93	1176	54.5
H.R.	2.9	40	35.5	31	87	1176	52
ANN	2.3	40	33.5	32.5	97	1078	53
Q/T	2.3	40	33.5	26	78	1078	57
H.R.	2.3	40	33.5	23	69	1078	53.5
ANN	1.5	15	37.8	29	77	996	55
Q/T	1.5	15	37.8	25.5	67	996	53
H.R.	1.5	15	37.8	28.5	75	996	51.5
ANN	1.7	15	52.9	53	100	1126	54
Q/T	1.7	15	52.9	34	64	1126	54
H.R.	1.7	15	52.9	42	79	1126	51
ANN	2.8	60	14.6	22	151	931	54.5
Q/T	2.8	60	14.6	13	89	931	51.5
H.R.	2.8	60	14.6	12.5	86	931	52.5
ANN	1.9	10	86.1	83.5	97	1353	53.5
Q/T	1.9	10	86.1	73	85	1353	50.5
H.R.	1.9	10	86.1	72	84	1353	51
ANN	1.4	5	91.0	104	114	1238	53
Q/T	1.4	5	91.0	71.5	79	1238	51.5
H.R.	1.4	5	91.0	81.5	90	1238	49.5

95.5% OF THEORETICAL
STANDARD DEVIATION
29.0%

SAE 8620

α = 0.05 cm^2/sec

T_T = 840° C

CONDITION	POWER (kW)	SPEED (in/min)	CALCULATED CASE (mil)	MEASURED CASE (mil)	% OF THEORETICAL	CALCULATED SURFACE TEMP. (C°)	SURFACE HARDNESS (Rc)
Q/T	2.3	40	12	15	125	965	41
ANN	2.3	40	12	7	58	965	45
Q/T	2.0	30	14.2	21	148	969	41
ANN	2.0	30	14.2	12.5	88	969	38
Q/T	2.4	30	30.9	33	107	1159	40
ANN	2.4	30	30.9	31	100	1159	46.5
Q/T	1.6	15	36.3	34	94	1094	39
ANN	1.6	15	36.3	23	63	1094	44.5
Q/T	1.4	5	74.7	67.5	90	1258	41.5
ANN	1.4.	5	74.7	63.5	85	1258	43.5
Q/T	2.9	60	11.7	16	137	993	40.5
ANN	2.9	60	11.7	6	51	993	37.5

102.5% OF THEORETICAL
STANDARD DEVIATION
25.9%

HYTEN B 3X

$\alpha = 0.049\ cm^2/sec$

$T_T = 760°\ C$

CONDITION	POWER (kW)	SPEED (in/min)	CALCULATED CASE (mil)	MEASURED CASE (mil)	% OF THEORETICAL	CALCULATED SURFACE TEMP. (C°)	SURFACE HARDNESS (Rc)
Q/T	2.8	60	10.8	13	120	888	56.5
ANN	2.8	60	10.8	6	56	888	55.5
Q/T	2.2	40	10.2	15	147	855	57
ANN	2.2	40	10.2	11	108	855	55
Q/T	2.8	40	29.1	32	110	1083	57
ANN	2.8	40	29.1	33	113	1083	57.5
Q/T	3.5	40	45.4	44.5	98	1349	57.5
ANN	3.5	40	45.4	43.5	96	1349	58
Q/T	2.9	30	48.8	44	90	1242	56
ANN	2.9	30	48.8	43	88	1242	56.6

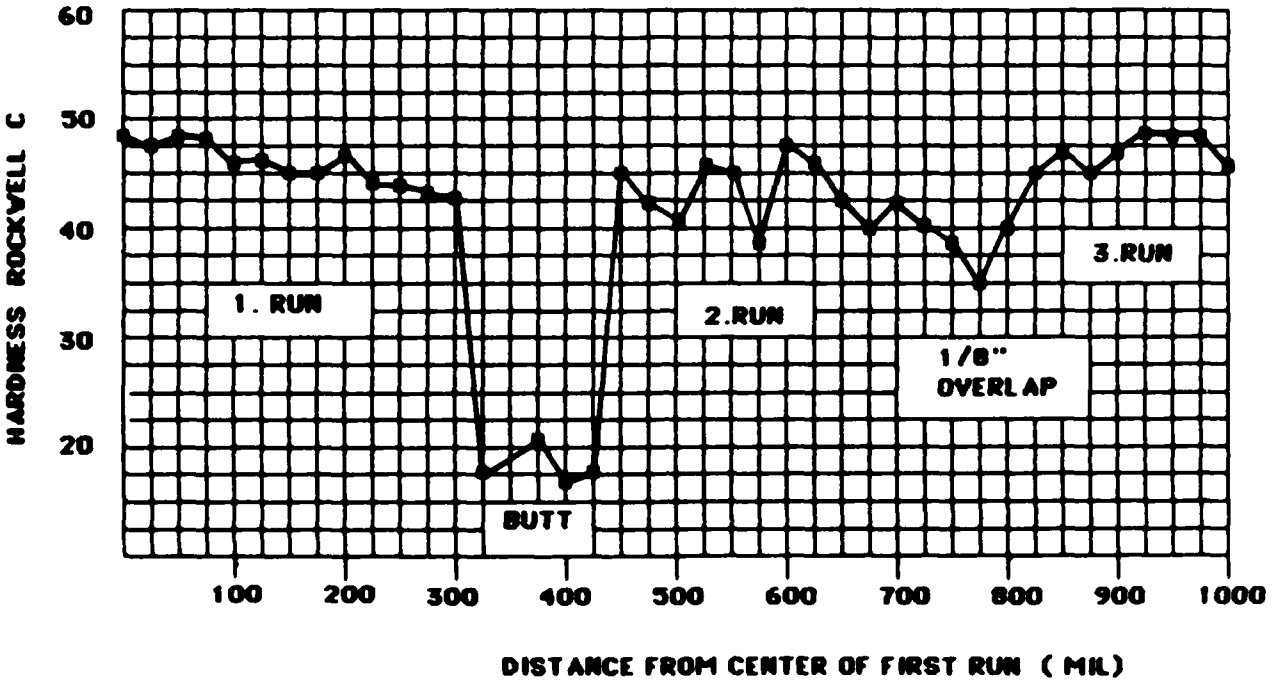

FIGURE 9.

SAE 8620 (HOT ROLLED). LASER HARDENED AT 1.4 Kv AND 5 IN/MIN PROCESSING SPEED.

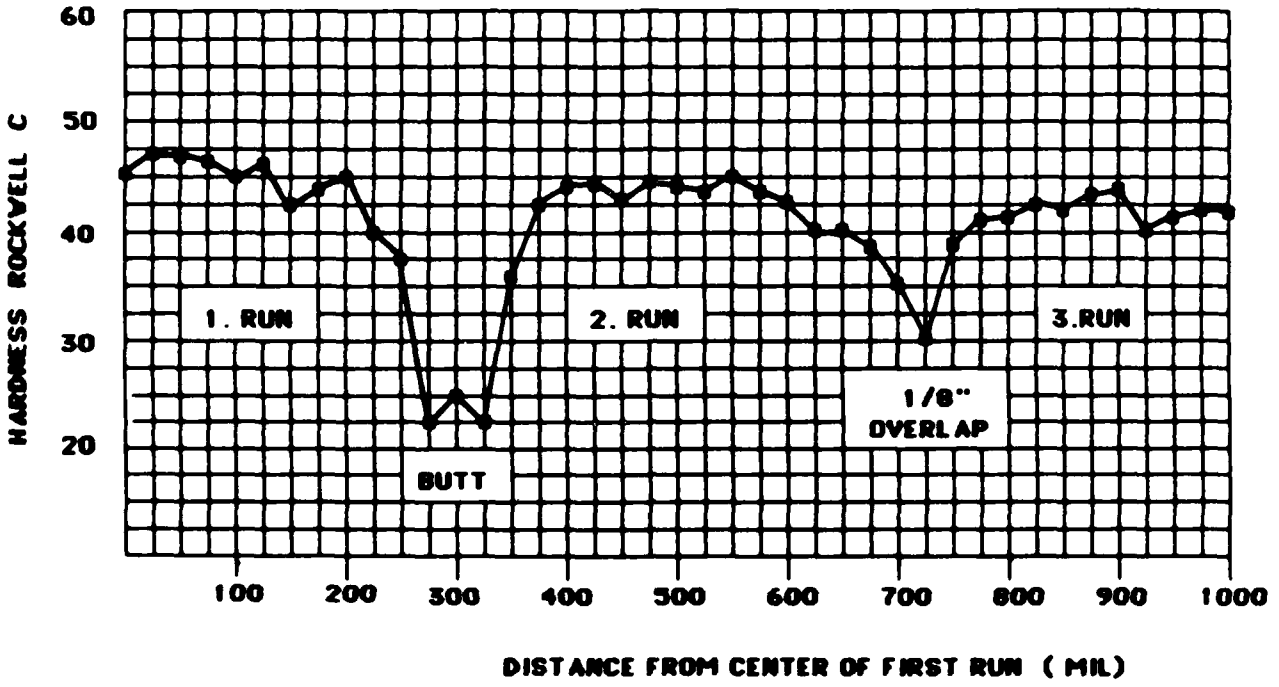

FIGURE 10.

SAE 8620 (QUENCHED AND TEMPERED). LASER HARDENED AT 1.4 Kw AND 5 IN/MIN PROCESSING SPEED.

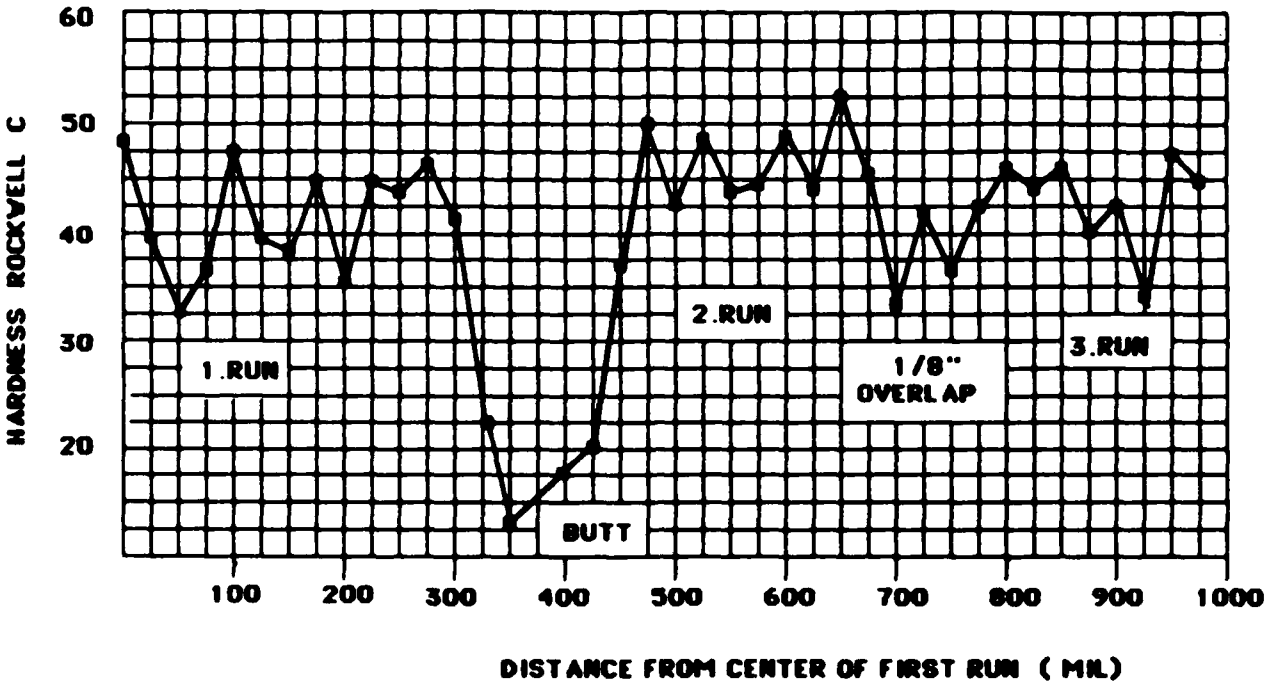

FIGURE 11.

SAE 8620 (HOT ROLLED). LASER HARDENED AT 2.4 Kw
AND 30 IN/MIN PROCESSING SPEED.

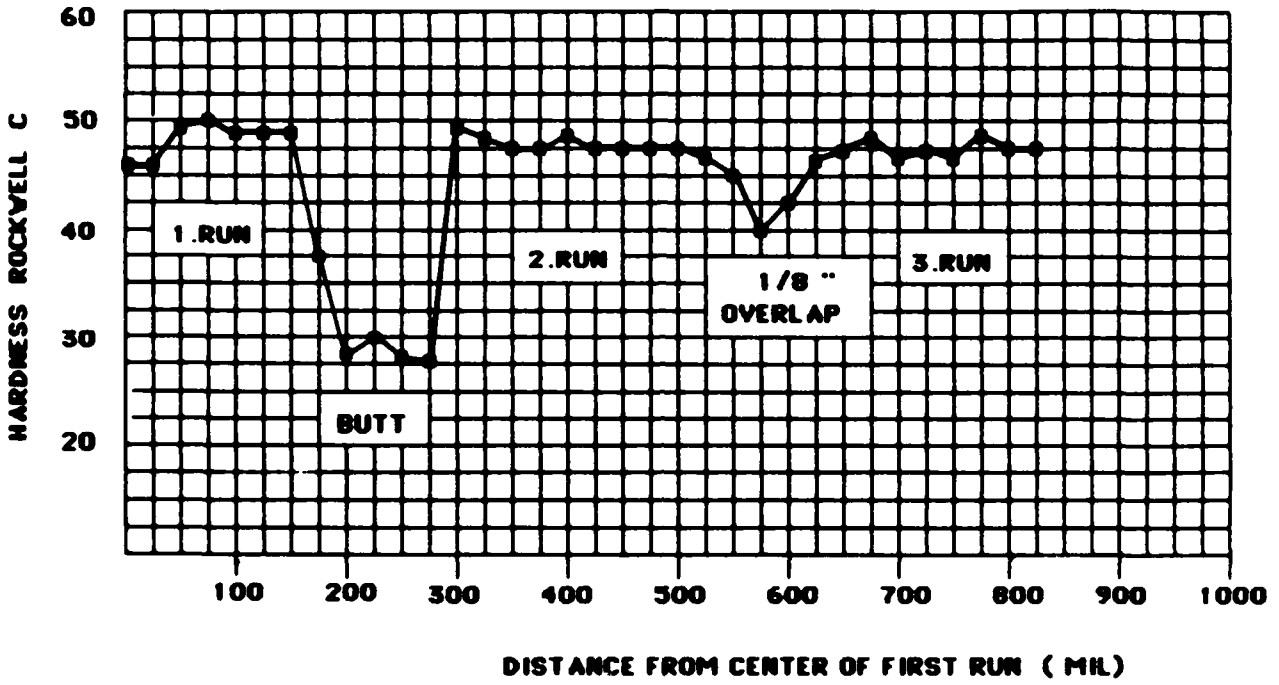

FIGURE 12.

SAE 8620 (QUENCHED AND TEMPERED). LASER HARDENED AT 2.4 Kw AND 30 IN/MIN PROCESSING SPEED.

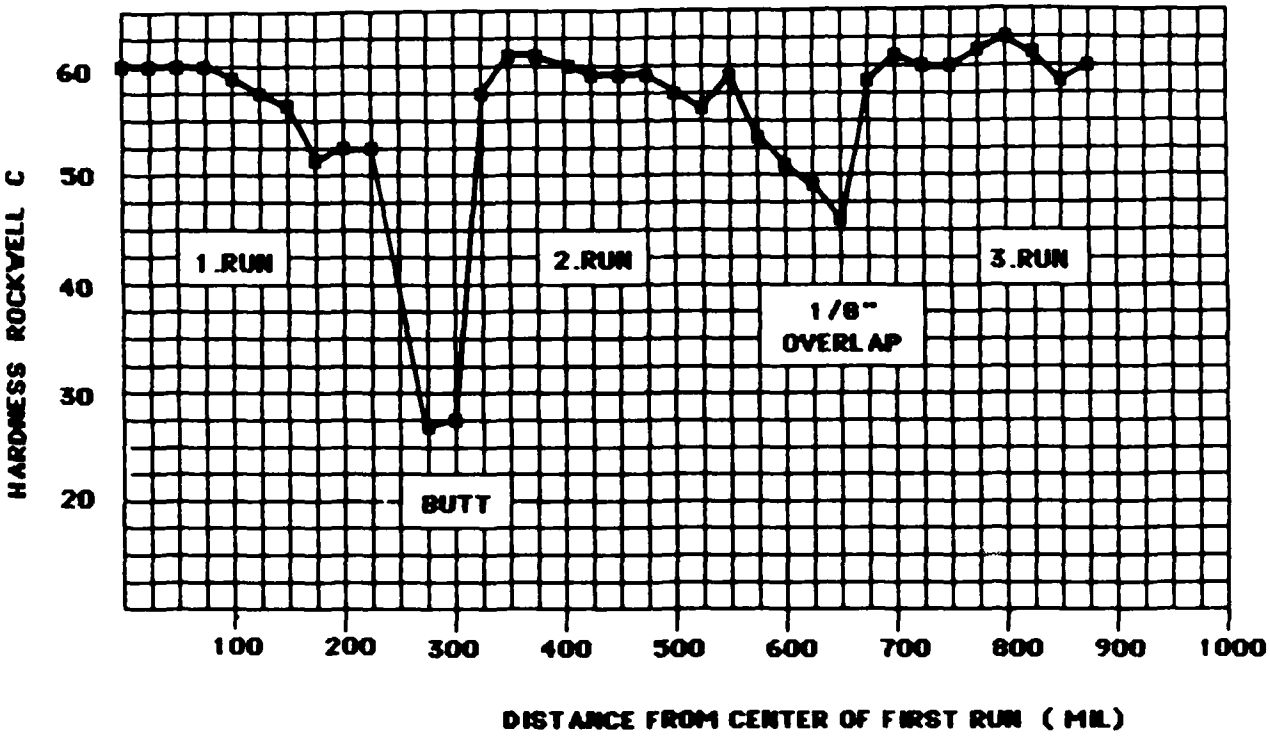

FIGURE 13.

HYTEN B 3X (QUENCHED AND TEMPERED). LASER HARDENED AT 1.2 Kw AND 5 IN/MIN PROCESSING SPEED.

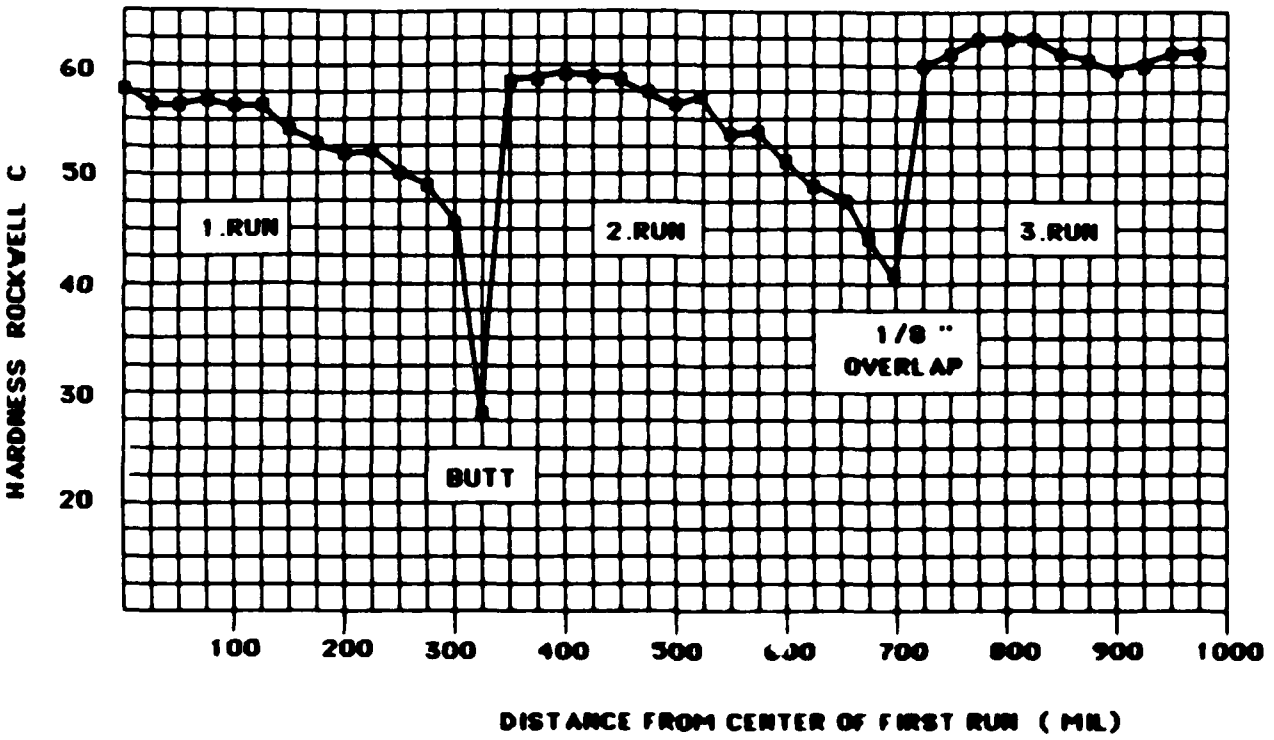

FIGURE 14

HYTEN B 3X (QUENCHED AND TEMPERED). LASER HARDENED AT 1.6 Kw AND 5 IN/MIN PROCESSING SPEED.

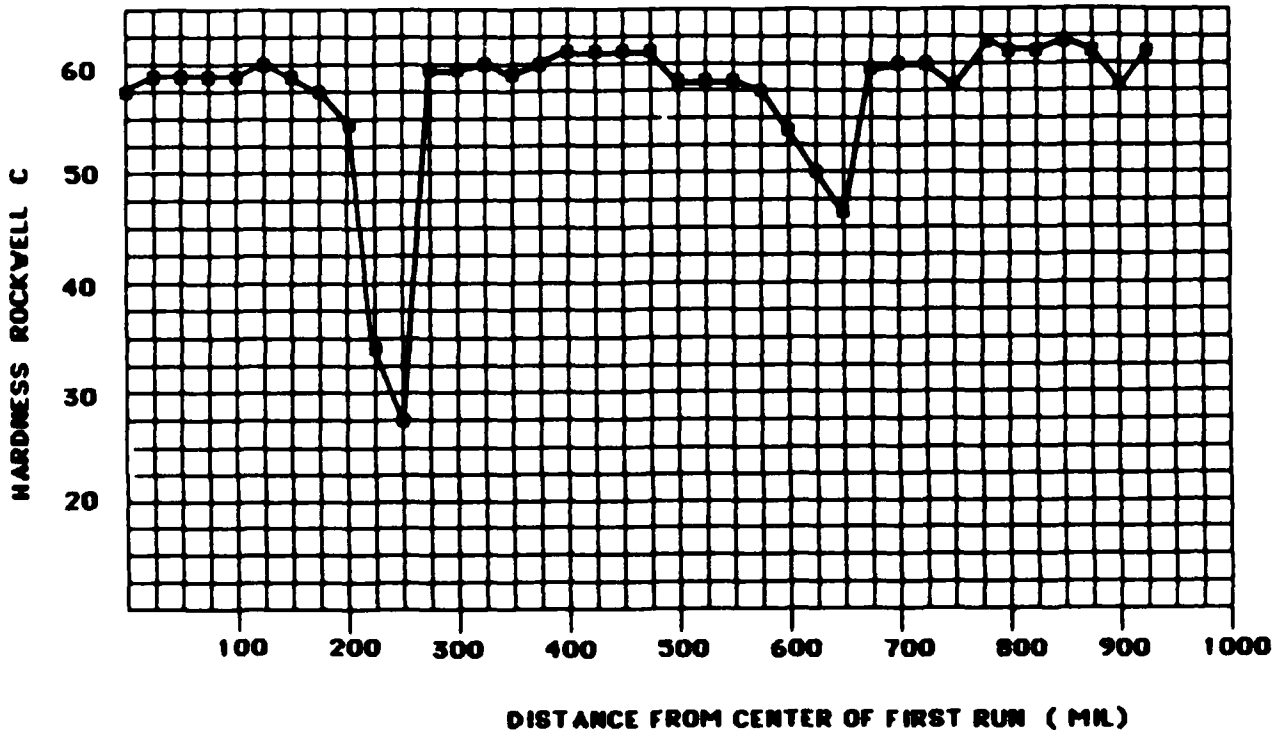

FIGURE 15.

HYTEN B 3X (QUENCHED AND TEMPERED).LASER HARDENED
AT 2.9 Kw AT 30 IN/MIN PROCESSING SPEED.

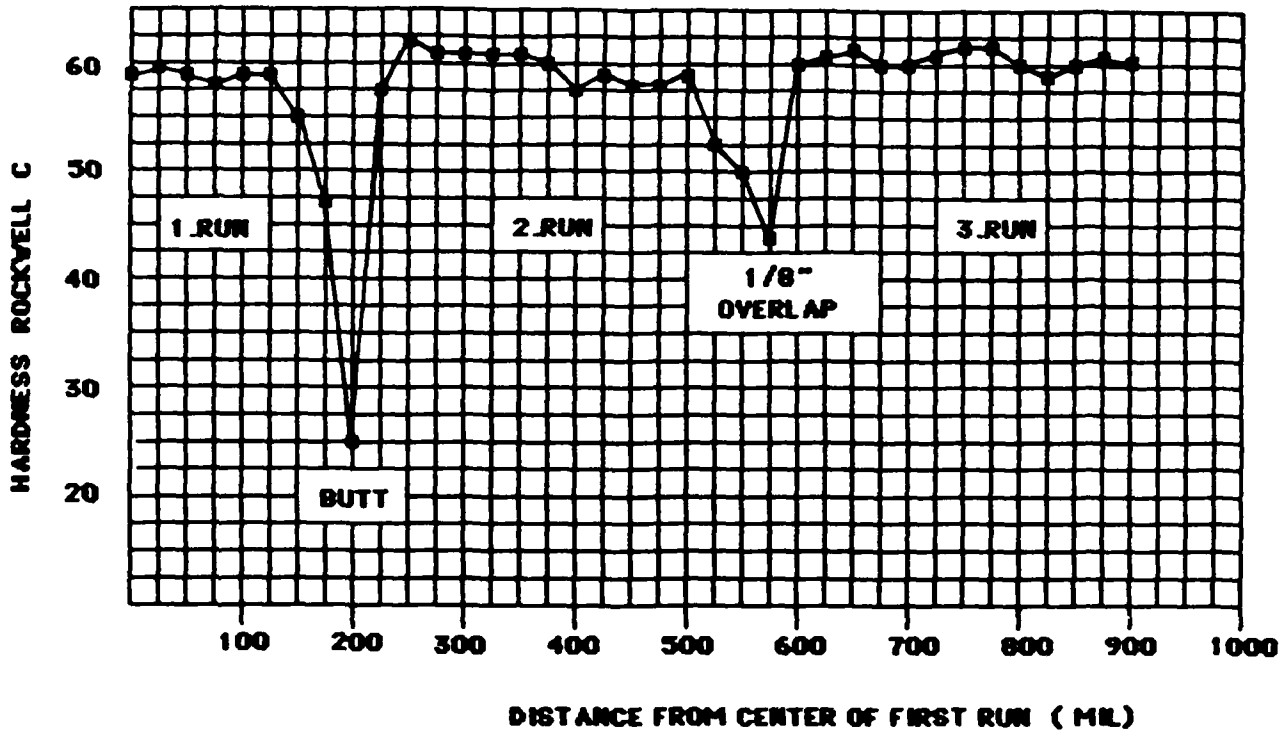

FIGURE 16.

HYTEN B 3X (QUENCHED AND TEMPERED). LASER HARDENED AT 2.9 Kw AND 40 IN/MIN PROCESSING SPEED.

interior. It is, however, possible that the surface will tend to contain a higher percentage of retained austenite than the interior, due to the very high temperature reached here during the laser processing. If this is the case, one should perhaps expect a more pronounced softening at low speed/high surface temperature, but this effect may be counteracted by the lower cooling rate occurrence in such cases. An answer to this question could, however, easily be obtained by X ray analysis.

- Overlap results show that positive overlap results in backtempering, but not to the bulk hardness of the material. From the point of view of hardness only, it is clearly more efficient to run overlap rather than butt to butt.

The 1020 samples provided by FMC did not develop an adequate hardened case under any combination of speed and power. From metallographic examination, it appeared that a slight decarburization had occurred at the surface, but removal of 50 mil of material by milling did not improve the hardenability of the material. A 1020 sample from Avco stock was processed for comparison purposes, and this material did harden, as expected. Figure 17 shows the hardness tracks obtained on these two materials at 2.9 kW power and 30 in/min speed. Figures 18 and 19 show the microstructure of the two materials. It is apparent that the grain size of the two materials is different, the FMC sample having the larger grain size; while there appears to be little difference in carbon content between the two. It is, therefore, reasonable to assume that the interaction time available in laser processing ($\sim$ 1 sec) is not sufficiently long to allow

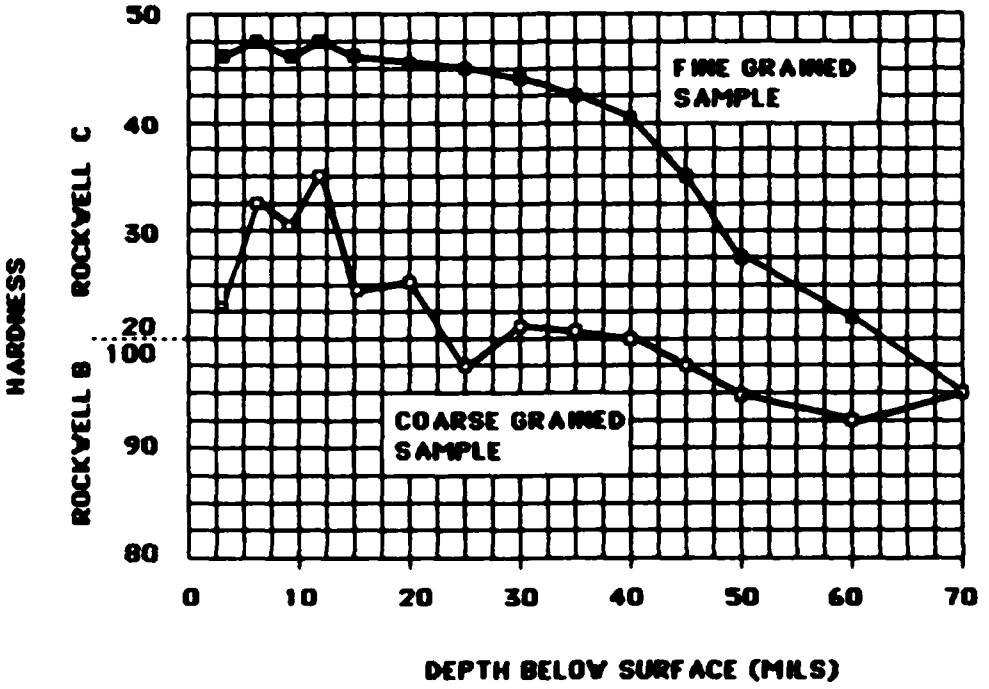

FIGURE 17.

HARDNESS PROFILES IN SAE 1020 STEELS, LASER HARDENED AT 2.9 Kw AND 30 IN/MIN PROCESSING SPEED.

FIGURE 18 STRUCTURE OF SAE 1020 (FMC)
500X

FIGURE 19 STRUCTURE OF SAE 1020 (AVCO)
500X

solution and redistribution of the carbon in the γ-phase to form a hardenable austenite in the coarse-grained material. Increased interaction time would give the longer carbon diffusion distances required for the coarse grained sample, but due to the low hardenability of 1020, the resulting self-quenching rates would not be sufficiently high to form 100% martensite. A profiled laser beam with "hot" leading edge would yield better results, but such a device was not available for this work.

The 4130 samples could not be laser processed with any benefit, since these samples already were in the fully hardened, untempered condition. (Bulk Hardness Rc 51). The only results of the laser processing are some softening at the surface, and tempering of the material at the bottom of the heat-affected zone.

3. CLADDING OF CATAPULT RAIL BARS

3.1 Objective

The objective of this phase of the program was to determine the feasibility of laser cladding carrier catapult rails with wear-resistant alloys, and to develop preliminary processing parameters and procedures for such cladding. Specifically, it was desired to develop methods for cladding the rail material with hardfacing alloys having approximately the same hardness as the substrate (approximately Rockwell C 32). Furthermore, the cladding process should be such that sharp edges could be maintained on the finished product. The final objective was to produce representative samples of cladded rail sections.

3.2 Experimental Work

3.2.1. Materials

Sample rails of two different types were provided by FMC/NOD. These consisted of bars made from SAE 4140 and Hy-90 steel, having cross-sectional dimensions 1 1/2" x 2". Two of the rail samples had been flame-sprayed with Stellite #6 E on one face. The other rails were uncoated.

For the laser cladding of the rails, three different types of hardfacing powder were provided. These consisted of Deloro 22, Deloro 35 and Stellite #6 E. In addition, 304 stainless steel powder for dilution of the hardfacing alloys was provided, in order to allow control of the cladding hardness and to lower cracking susceptibility where needed.

3.2.2. Equipment and Procedures

The laser processing was performed with an Avco HPL®-10 CO_2 laser with CW output. The laser output beam

was shaped with a square beam by means of an optical integrator, as shown in Figure 1. This beam had dimensions 1/2" x 1/2" in the focal plane. The entire experimental arrangement was essentially identical to the setup used for the heat treatment work discussed in Chapter 2 in this report and shown in Figure 2, with the addition of an argon gas blanket nozzle aimed at the laser spot from the trailing edge side of the spot.

The object of this gas blanket was to protect the molten material in the interaction zone from reaction with the ambient atmosphere. The gas flow through the nozzle was 15 fe^3/hr.

The alloy powder was preplaced onto the substrate surface, using 1/16" thick templates to obtain even coverage. Originally, it was the intention to use an automatic powder feeder for delivery of the alloy powder to the substrate, but the alloy powder used in this work did not flow well through this feeder. In particular, the stainless steel powder created problems due to its small grain size (+ 10 μm).

3.2.3. Development of Processing Parameters

Trial runs were made with all three powders at various power levels and processing speeds, ranging from 3 kW/cm^2 to 6 kW/cm^2 and 0.211 cm/sec to 0.847 cm/sec (5 in/min to 20 in/min). Both straight alloy powders and alloy powders with various amounts of 304 stainless steel powder added were clad onto 1/2" SAE 4140 steel plates.

It quickly became clear that the Stellite powder needed about 40% stainless steel addition, both to prevent cracking and to lower the hardness to an acceptable level. At this stage, no cracking problem was experienced

with Deloro 22 and Deloro 35. However, stainless steel addition to these two alloys resulted in a clad layer with variable hardness.

Because of this, it was decided to process the two Deloro alloys without stainless steel addition, even though the resulting clad layer had a hardness somewhat in excess of Rockwell C 32.

The following processing parameters gave the best combination of smooth flow, minimal dilution with the substrate, and absence of porosity.

STELLITE #6 E + 40% STAINLESS STEEL	
4.65 kW/cm^2	10 in/min
DELORO 22	
4.65 kW/cm^2	8 in/min
DELORO 35	
4.65 kW/cm^2	10 in/min

Following the determination of the optimal processessing parameters, overlapping runs were made (1/8" overlap). No problems with cracking or flow were encountered at this stage, but a tendency for pore formation in the Deloro 35 specimens in the overlap zone was noticed. These pores were predominantly in the surface region and did not appear to be of critical importance.

Finally, processing of the flame-sprayed test bars was attempted. This was not a success because the only effect of the laser processing, over a wide range of power and speed, was erosion of the sprayed layer. At power input rates sufficiently high to cause any reaction whatsoever, a veritable shower of sparks was generated. This gave the impression that the sprayed layer was under intense residual stresses.

3.2.4. Edge Control

In order to obtain sharp edges on the clad bars, both at the ends and along the edges, a series of runs were made to find a way to obtain this. The following techniques were found to give satisfactory results.

- To obtain sharp edges at the ends of the bars, two short pieces were cut from the barstock and used as run-on and run-off pieces. The fitup of these pieces must be good enough to allow cladding across the gap without any loss of powder through the gap. If necessary, the gap could be sealed off with a slurry of the alloy powder. (Alcohol or Nicobraze can be used as a carrier). By starting the cladding at least an inch past the end-gap, a continuous clad deposit could be made. After laser processing, the end-pieces could be knocked off cleanly, or cut by sawing or abrasive wheel.

- To obtain sharp edges along the bar, stainless steel extension surfaces were used. These consisted of 1/16" stainless (304) plates fitting tightly along the edges. These plates were clamped down on another steel bar to provide heat-sinking. It is important that the extension surface is as long as the bar plus the two end pieces, otherwise through-melting will result at the corners. The edge cladding was performed with about half the width of the final run on the bar and the other half on the extension surface. After processing, the stainless steel plate could be cut from the underside, providing a sharp edge. Figure 20 shows the technique of edge control.

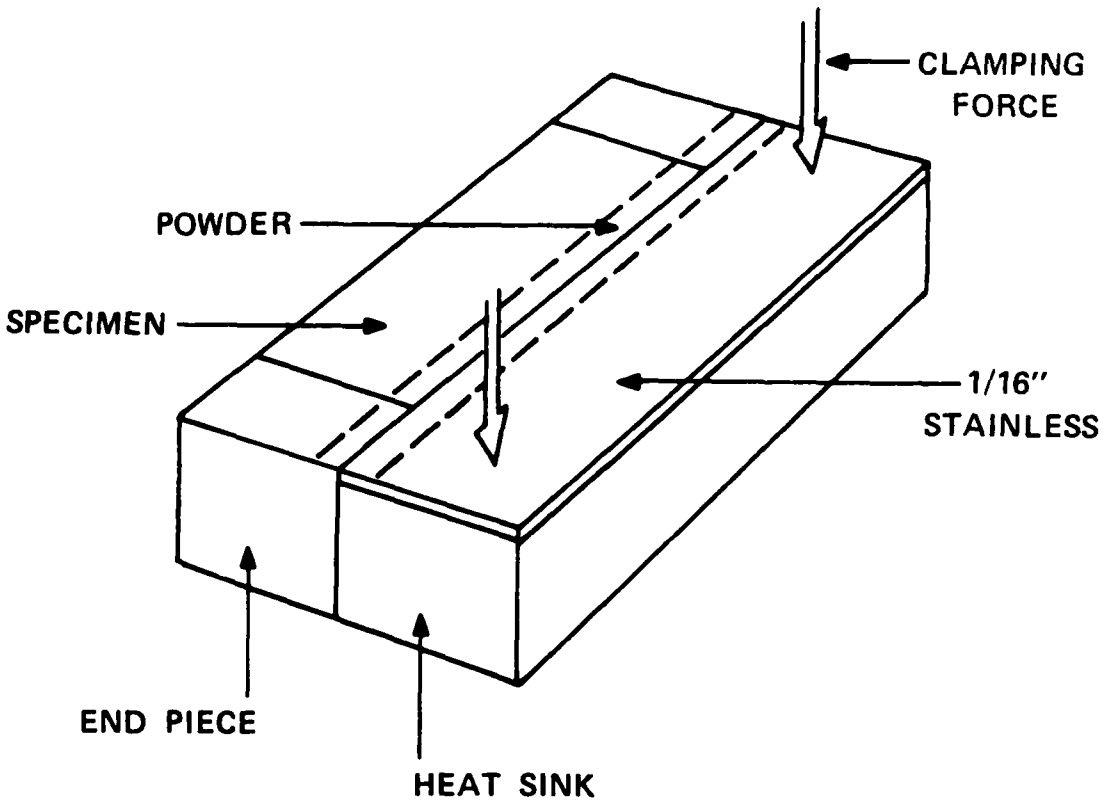

FIGURE 20 EDGE CONTROL IN LASER CLADDING

3.2.5. Preparation of Specimens

Six specimens, each about 2.5" long, were cut from the 1 1/2" x 2" bars, three from SAE 4140 bars and three from Hy-90 bars. These were clad on one of the 1 1/2" faces, using overlapping runs and edge control techniques (as described above) to obtain uniform cladding of about 0.05" thickness over the entire surface. Each of the three alloys were clad onto both SAE 4140 and Hy-90 substrates. Figure 21 shows the shape of the final specimens. (Deloro 22 on SAE 4140).

3.3 Results and Discussion

Both the Stellite #6 E + 40% stainless steel specimens developed cracks at the third overlay pass. These cracks were of the "herring bone" type. The Deloro 35 specimens also showed cracks in the third overlay, but these were normal to the processing direction. In order to prevent cracking, new specimens were made as before, but with stress relief between each cladding run (1200°F for 1 hour). No improvement was observed in the Stellite #6 E specimens, but one of the Deloro 35 (on SAE 4140) was apparently crack-free. Deloro 35 on Hy-90, however, showed the cracks.

The two Deloro 22 specimens showed no cracks, and these were not stress-relieved between runs.

Figures 22 through 24 show the hardness profiles of the six different cladded specimens. In all cases, the clad layer is 45 to 50 mil deep, with a hardness ranging from 32 to 42 Rockwell C. The substrates of the specimens cladded with Deloro 22 show transformation hardening in the vicinity of the clad/substrate interface. This is absent in the other specimens, due to the stress-relief heat treatment.

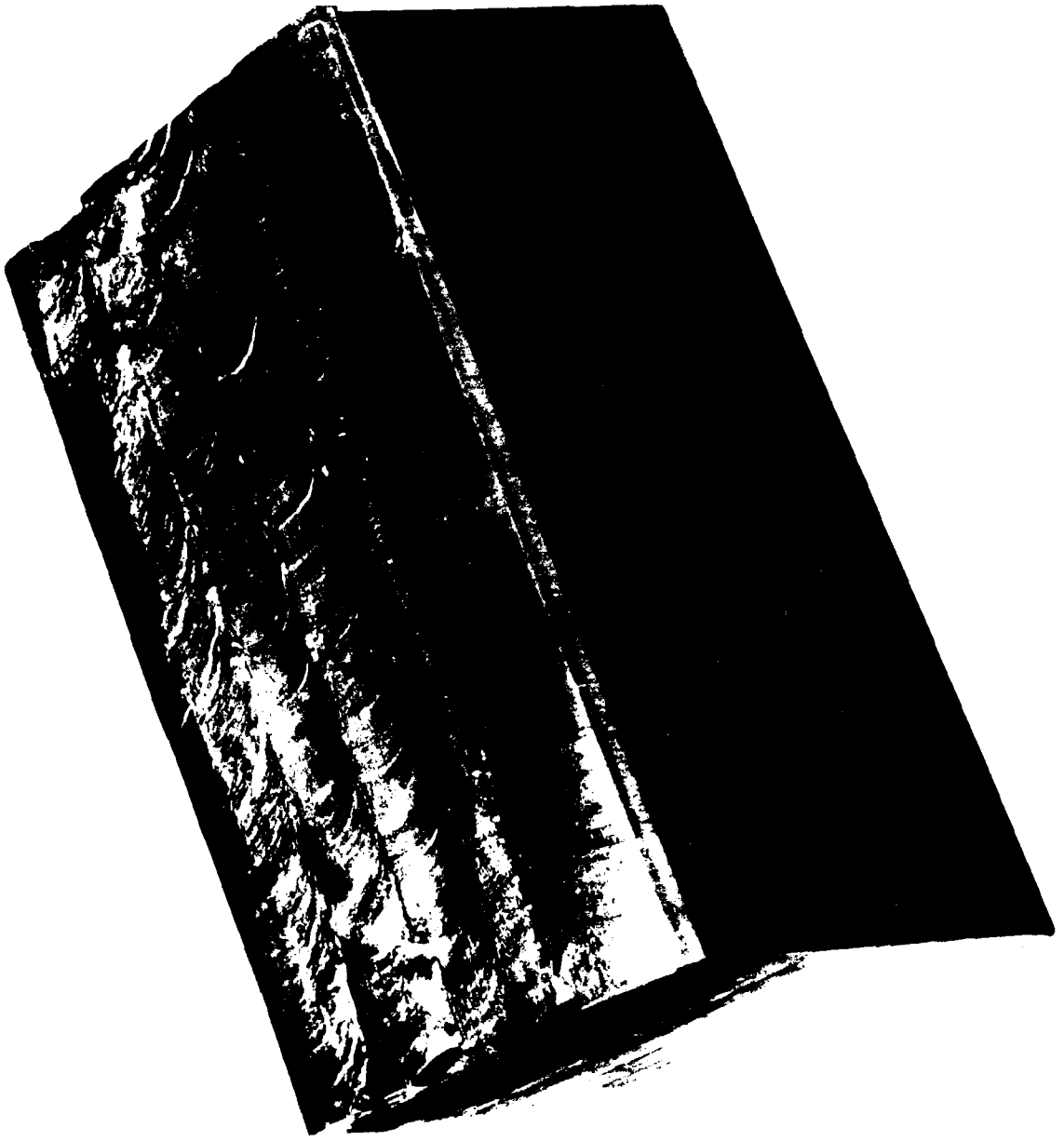

FIGURE 21 SAE 4140 STEEL BAR CLADDED WITH DELORO 22

Cladding of catapult rails with Deloro 22 can be performed easily. The hardness of the overlay is Rockwell C 35 to 40. The 4140 substrate shows transformation hardening to a peak hardness of Rc 51-52. The Hy-90 substrate does not harden to more than Rc 40.

The Deloro 35 and Stellite #6 E alloys can probably not be clad onto these steels in a continuous manner without preheating and slow post-processing cooling to prevent cracking.

Remelting of flame-sprayed layers was not successful in this case, but this should be possible if closer control of the spraying process is exercised.

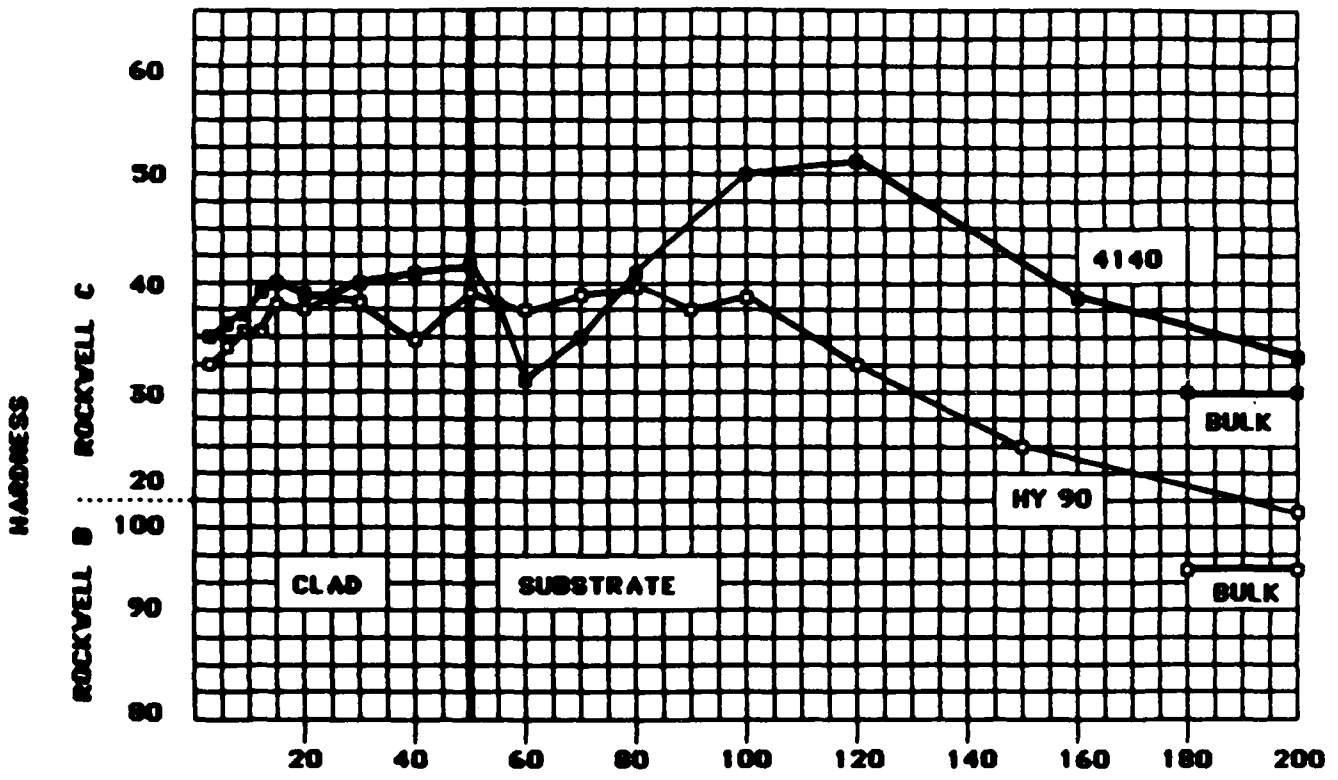

FIGURE 22.

DELORO 22. LASER CLADDED AT 4.65 Kw/cm^2
AND 0.339 cm/sec PROCESSING SPEED.

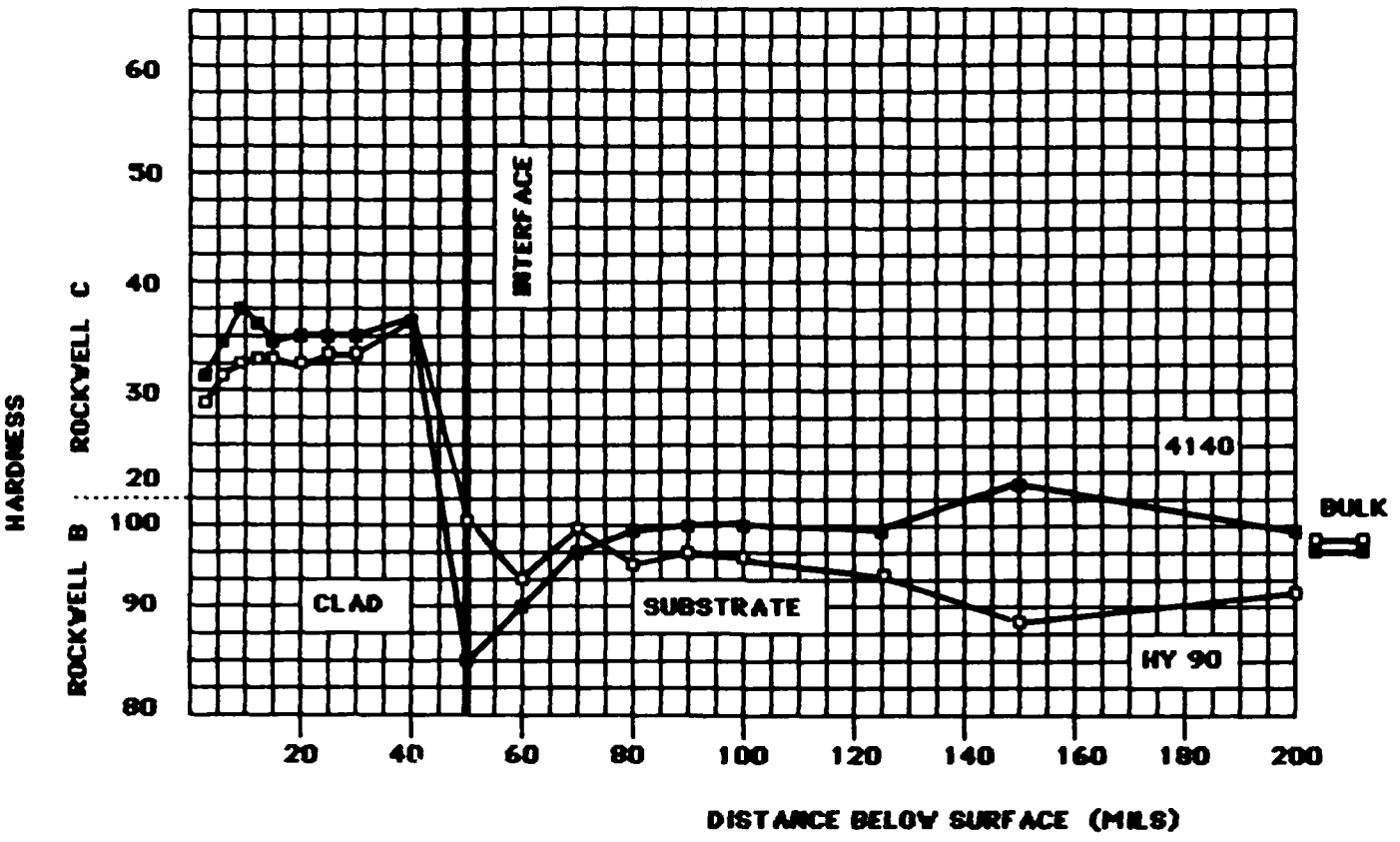

FIGURE 23

STELLITE 6 E + 40% STAINLESS STEEL, LASER CLADDED AT 4.65 Kw/cm^2 AND 0.423 cm/sec PROCESSING SPEED.

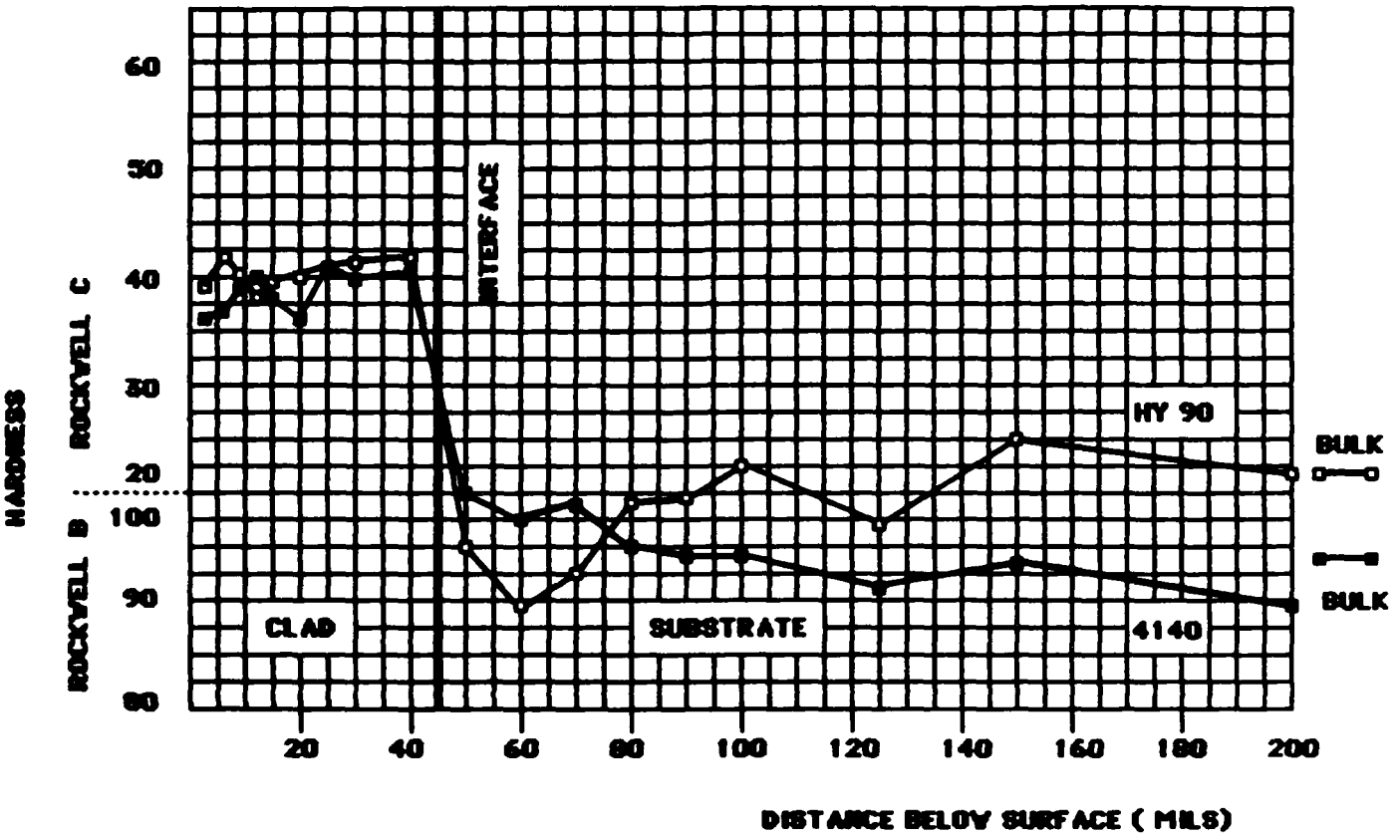

FIGURE 24.

DELORO 35. LASER CLADDED AT 4.65 Kv/cm^2
AND 0.423 cm/sec PROCESSING SPEED.

LIST OF REFERENCES

1) Rose, A., and Strassburg, V. (1956). Stahl and Eisen, 76, No. 15. 976-983.

2) Sandven, O.A. (1981). Laser Surface Heat Treatment With Profiled Beams. Proc. International Laser Conf., Anaheim, CA.

3) Carslaw, H.S. and Jaeger, J.C. (1959). Conduction of Heat in Solids. Oxford Press, 2nd ed. 75.

4) ibid. 270.

5) Sandven, O.A. (1983). Three-Dimensional Heat Flow Model for Prediction of Case Depth in Laser Surface Transformation Hardening. ICALEO Conf., Los Angeles, CA.

6) ASM METALS HANDBOOK, 9th Ed. (1978). Vol. 1: 145-151.

APPENDIX I

The program listed on the following pages is based on the one-dimensional heat flow model and should not be used for low processing speed.

The program is written for use on a Texas Instrument TI 59 programmable calculator with a PC-100C printer.

User Instructions

1. Partition the calculator to mode 714:29 by entering 3 and push 2th op. 17.
2. Enter power density in A (w/cm^2).
3. Enter speed in B (cm/sec).
4. Enter spot length in C (cm).
5. Enter thermal conductivity and press R/S (w/cmC°).
6. Enter thermal diffusivity and press R/S (cm^2/sec).
7. Enter room temperature in D (C°).
8. Enter transition temperature and press R/S (c°).
9. Execute program by pressing A^1.

The calculator will print dwelltime, surface temperature and case depth. If the heat input is insufficient to form any case, "NO CASE" is printed. If the processing speed is too low for this model, "USE 3-D" will be printed.

If cooling rates behind the laser spot are desired, enter the total time (dwelltime + cooling time combined) and press B^1. This must be done after the case depth has been calculated. The calculator will print surface temperature at the entered time, the rate of cooling (in c°/sec), the temperature at the bottom of the case and the rate of cooling at this point. The procedure can be repeated for any desired total time.

PROGRAM FOR PREDICTION OF CASE DEPTH

(One-Dimensional)

```
000  76 LBL
001  11  A
002  53  (
003  42 STO
004  00  00
005  65  ×
006  00  0
007  93  .
008  08  8
009  05  5
010  95  =
011  42 STO
012  10  10
013  54  )
014  92 RTN
015  76 LBL
016  12  B
017  53  (
018  42 STO
019  01  01
020  54  )
021  92 RTN
022  76 LBL
023  13  C
024  53  (
025  42 STO
026  02  02
027  91 R/S
028  42 STO
029  03  03
030  91 R/S
031  42 STO
032  04  04
033  54  )
034  92 RTN
035  76 LBL
036  14  D
037  53  (
038  42 STO
039  05  05
040  91 R/S
041  42 STO
042  06  06
043  54  )
044  92 RTN
045  76 LBL
046  16 A'
047  53  (
048  43 RCL
049  02  02
050  55  ÷
051  43 RCL
052  01  01
053  95  =
054  42 STO
055  07  07
056  25 CLR
057  69 DP
058  00  00
059  01  1
060  06  6
061  04  4
062  03  3
063  01  1
064  07  7
065  02  2
066  07  7
067  02  2
068  07  7
069  69 DP
070  01  01
071  69 DP
072  05  05
073  43 RCL
074  07  07
075  99 PRT
076  01  1
077  06  6
078  65  ×
079  43 RCL
080  04  04
081  55  ÷
082  43 RCL
083  01  01
084  95  =
085  32 X:T
086  43 RCL
087  02  02
088  77  GE
089  01  01
090  13  13
091  25 CLR
092  69 DP
093  00  00
094  04  4
095  01  1
096  03  3
097  06  6
098  01  1
099  07  7
100  69 DP
101  01  01
102  00  0
103  04  4
104  02  2
105  00  0
106  01  1
107  06  6
108  69 DP
109  02  02
110  69 DP
111  05  05
112  92 RTN
113  02  2
114  65  ×
115  43 RCL
116  10  10
117  55  ÷
118  43 RCL
119  03  03
120  65  ×
121  53  (
122  43 RCL
123  04  04
124  65  ×
125  43 RCL
126  07  07
127  55  ÷
128  89  π
129  54  )
130  34 FX
131  85  +
132  43 RCL
133  05  05
134  95  =
135  42 STO
136  08  08
137  43 RCL
138  06  06
139  32 X:T
140  43 RCL
141  08  08
142  77  GE
143  01  01
144  68  68
145  25 CLR
146  69 DP
147  00  00
148  03  3
149  01  1
150  02  2
```

PROGRAM FOR PREDICTION OF CASE DEPTH

(One-Dimensional)

```
151  02   2
152  69 DP
153  01   01
154  01   1
155  05   5
156  01   1
157  03   3
158  03   3
159  06   6
160  01   1
161  07   7
162  69 DP
163  02   02
164  69 DP
165  05   05
166  54   )
167  92 RTN
168  25 CLR
169  69 DP
170  00   00
171  03   3
172  06   6
173  04   4
174  01   1
175  03   3
176  05   5
177  02   2
178  01   1
179  69 DP
180  01   01
181  03   3
182  07   7
183  01   1
184  07   7
185  03   3
186  00   0
187  03   3
188  03   3
189  69 DP
190  02   02
191  69 DP
192  05   05
193  43 RCL
194  08   08
195  59 INT
196  99 PRT
197  02   2
198  65   ×
199  43 RCL
200  10   10
201  55   ÷
202  43 RCL
203  03   03
204  65   ×
205  53   (
206  43 RCL
207  04   04
208  65   ×
209  43 RCL
210  07   07
211  54   )
212  34 fX
213  95   =
214  42 STO
215  11   11
216  02   2
217  65   ×
218  53   (
219  43 RCL
220  04   04
221  65   ×
222  43 RCL
223  07   07
224  54   )
225  34 fX
226  95   =
227  42 STO
228  12   12
229  00   0
230  42 STO
231  13   13
232  00   0
233  93   .
234  00   0
235  05   5
236  42 STO
237  14   14
238  43 RCL
239  13   13
240  85   +
241  43 RCL
242  14   14
243  95   =
244  42 STO
245  13   13
246  55   ÷
247  43 RCL
248  12   12
249  95   =
250  10 E'
251  65   ×
252  43 RCL
253  11   11
254  85   +
255  43 RCL
256  05   05
257  95   =
258  42 STO
259  15   15
260  43 RCL
261  15   15
262  75   -
263  43 RCL
264  06   06
265  95   =
266  50 I×I
267  32 X:T
268  01   1
269  77   GE
270  03   03
271  31   31
272  43 RCL
273  06   06
274  32 X:T
275  43 RCL
276  15   15
277  77   GE
278  03   03
279  14   14
280  86 STF
281  01   01
282  43 RCL
283  14   14
284  55   ÷
285  02   2
286  95   =
287  42 STO
288  14   14
289  43 RCL
290  13   13
291  75   -
292  43 RCL
293  14   14
294  95   =
295  42 STO
296  13   13
297  55   ÷
298  43 RCL
299  13   13
300  95   =
```

PROGRAM FOR PREDICTION OF CASE DEPTH

(One-Dimensional)

```
301  10 E'
302  65  ×
303  43 RCL
304  11  11
305  85  +
306  43 RCL
307  05  05
308  95  =
309  42 STO
310  15  15
311  61 GTO
312  02  02
313  60  60
314  87 IFF
315  01  01
316  03  03
317  21  21
318  61 GTO
319  02  02
320  38  38
321  43 RCL
322  14  14
323  55  ÷
324  02  2
325  95  =
326  42 STO
327  14  14
328  61 GTO
329  02  02
330  38  38
331  25 CLR
332  69 DP
333  00  00
334  01  1
335  05  5
336  01  1
337  03  3
338  03  3
339  06  6
340  01  1
341  07  7
342  69 DP
343  01  01
344  69 DP
345  05  05
346  43 RCL
347  13  13
348  99 PRT
349  93 ADV
350  22 INV
351  86 STF
352  01  01
353  54  )
354  92 RTN
355  76 LBL
356  17 B'
357  53  (
358  42 STO
359  16  16
360  02  2
361  65  ×
362  43 RCL
363  10  10
364  55  ÷
365  43 RCL
366  03  03
367  65  ×
368  43 RCL
369  04  04
370  34 ΓX
371  95  =
372  42 STO
373  17  17
374  43 RCL
375  17  17
376  65  ×
377  53  (
378  43 RCL
379  16  16
380  55  ÷
381  89  π
382  54  )
383  34 ΓX
384  95  =
385  42 STO
386  18  18
387  43 RCL
388  17  17
389  65  ×
390  53  (·
391  53  (
392  43 RCL
393  16  16
394  75  -
395  43 RCL
396  07  07
397  54  )
398  55  ÷
399  89  π
400  54  )
401  34 ΓX
402  95  =
403  42 STO
404  19  19
405  43 RCL
406  18  18
407  75  -
408  43 RCL
409  19  19
410  85  +
411  43 RCL
412  05  05
413  95  =
414  42 STO
415  20  20
416  59 INT
417  99 PRT
418  53  (
419  43 RCL
420  08  08
421  75  -
422  43 RCL
423  20  20
424  54  )
425  55  ÷
426  53  (
427  43 RCL
428  16  16
429  75  -
430  43 RCL
431  07  07
432  54  )
433  95  =
434  59 INT
435  99 PRT
436  43 RCL
437  13  13
438  55  ÷
439  02  2
440  55  ÷
441  53  (
442  43 RCL
443  04  04
444  65  ×
445  43 RCL
446  16  16
447  54  )
448  34 ΓX
449  95  =
450  10 E'
```

PROGRAM FOR PREDICTION OF CASE DEPTH

(One-Dimensional)

```
451  65  ×
452  43 RCL
453  17  17
454  65  ×
455  43 RCL
456  16  16
457  34 ΓX
458  95  =
459  42 STO
460  21  21
461  43 RCL
462  13  13
463  55  ÷
464  02  2
465  55  ÷
466  53  (
467  43 RCL
468  04  04
469  65  ×
470  53  (
471  43 RCL
472  16  16
473  75  -
474  43 RCL
475  07  07
476  54  )
477  54  )
478  34 ΓX
479  95  =
480  10 E'
481  65  ×
482  43 RCL
483  17  17
484  65  ×
485  53  (
486  43 RCL
487  16  16
488  75  -
489  43 RCL
490  07  07
491  54  )
492  34 ΓX
493  95  =
494  42 STO
495  22  22
496  43 RCL
497  21  21
498  75  -
499  43 RCL
500  22  22

501  85  +
502  43 RCL
503  05  05
504  95  =
505  42 STO
506  23  23
507  59 INT
508  99 PRT
509  53  (
510  43 RCL
511  15  15
512  75  -
513  43 RCL
514  23  23
515  54  )
516  55  ÷
517  53  (
518  43 RCL
519  16  16
520  75  -
521  43 RCL
522  07  07
523  54  )
524  95  =
525  59 INT
526  99 PRT
527  54  )
528  92 RTN
529  76 LBL
530  10 E'
531  53  (
532  42 STO
533  24  24
534  04  4
535  32 X:T
536  43 RCL
537  24  24
538  77  GE
539  06  06
540  73  73
541  43 RCL
542  24  24
543  65  ×
544  00  0
545  93  .
546  03  3
547  02  2
548  07  7
549  05  5
550  03  3

551  01  1
552  01  1
553  85  +
554  01  1
555  95  =
556  35 1/X
557  42 STO
558  25  25
559  53  (
560  00  0
561  93  .
562  02  2
563  05  5
564  04  4
565  08  8
566  02  2
567  02  2
568  09  9
569  05  5
570  09  9
571  02  2
572  65  ×
573  43 RCL
574  25  25
575  75  -
576  00  0
577  93  .
578  02  2
579  08  8
580  04  4
581  04  4
582  09  9
583  06  6
584  07  7
585  03  3
586  06  6
587  65  ×
588  43 RCL
589  25  25
590  33 X²
591  85  +
592  01  1
593  93  .
594  04  4
595  02  2
596  01  1
597  04  4
598  01  1
599  03  3
600  07  7
```

PROGRAM FOR PREDICTION OF CASE DEPTH

(One-Dimensional)

601	04	4
602	01	1
603	65	×
604	43	RCL
605	25	25
606	45	Y^x
607	03	3
608	75	-
609	01	1
610	93	.
611	04	4
612	05	5
613	03	3
614	01	1
615	05	5
616	02	2
617	00	0
618	02	2
619	07	7
620	65	×
621	43	RCL
622	25	25
623	45	Y^x
624	04	4
625	85	+
626	01	1
627	93	.
628	00	0
629	06	6
630	01	1
631	04	4
632	00	0
633	05	5
634	04	4
635	02	2
636	09	9
637	65	×
638	43	RCL
639	25	25
640	45	Y^x
641	05	5
642	54	)
643	65	×
644	01	1
645	22	INV
646	23	LNX
647	45	Y^x
648	43	RCL
649	24	24
650	33	X²
651	94	+/-
652	95	=
653	42	STO
654	26	26
655	01	1
656	22	INV
657	23	LNX
658	45	Y^x
659	43	RCL
660	24	24
661	33	X²
662	94	+/-
663	55	÷
664	89	π
665	34	√X
666	75	-
667	43	RCL
668	24	24
669	65	×
670	43	RCL
671	26	26
672	85	+
673	00	0
674	95	=
675	54	)
676	92	RTN

APPENDIX II

The program listed on the following pages utilizes a one-dimensional heat flow model for the high speed range, and a three-dimensional model for the low speed ranges.

The program is written for use on a Texas Instrument TI 59. programmable calculator with a PC-100 printer.

User Instructions

1. Partition the calculator to mode 799:19 by entering 2 and push 2th op. 17.
2. Enter laser power (watts) in A.
3. Enter speed (cm/sec) in B.
4. Enter thermal conductivity (w/cmC°) in C.
5. Enter thermal diffusivity (cm^2/sec) in D.
6. Enter transformation temperature (C°) in E.
7. Enter size of laser spot (cm) in A^1.
8. Enter room temperature (c°) in B^1.
9. Press C^1. The value of the parameter $B = \nu b/2\alpha$ will be displayed. Now press R/S. The calculator will print surface temperature, depth of case (in cm and mils), the value of the parameter B and the ratio of the parameters Z and B ($Z = \nu z/2\alpha$). The results are valid if:

$$B \gtrsim 0.5$$

$$Z/B \lesssim 0.5 \text{ for } 1 \gtrsim B \gtrsim 0.5$$

$$Z/B \lesssim 0.4 \text{ for } 4 \gtrsim B \gtrsim 1$$

$$\text{for all values of } B \gtrsim 4$$

PROGRAM FOR PREDICTION OF CASE

(Three-Dimensional)

```
000  76 LBL
001  11  A
002  53  (
003  42 STO
004  00  00
005  54  )
006  92 RTN
007  76 LBL
008  12  B
009  53  (
010  42 STO
011  01  01
012  54  )
013  92 RTN
014  76 LBL
015  13  C
016  53  (
017  42 STO
018  02  02
019  54  )
020  92 RTN
021  76 LBL
022  14  D
023  53  (
024  42 STO
025  03  03
026  54  )
027  92 RTN
028  76 LBL
029  15  E
030  53  (
031  42 STO
032  04  04
033  54  )
034  92 RTN
035  76 LBL
036  16  A'
037  53  (
038  42 STO
039  05  05
040  54  )
041  92 RTN
042  76 LBL
043  17  B'
044  53  (
045  42 STO
046  06  06
047  54  )
048  92 RTN
049  76 LBL
050  18  C'
051  53  (
052  43 RCL
053  00  00
054  55  ÷
055  43 RCL
056  05  05
057  33  X²
058  65  ×
059  00  0
060  93  .
061  08  8
062  05  5
063  95  =
064  42 STO
065  07  07
066  43 RCL
067  05  05
068  55  ÷
069  43 RCL
070  01  01
071  95  =
072  42 STO
073  08  08
074  43 RCL
075  05  05
076  65  ×
077  43 RCL
078  01  01
079  55  ÷
080  04  4
081  55  ÷
082  43 RCL
083  03  03
084  95  =
085  42 STO
086  09  09
087  91 R/S
088  43 RCL
089  04  04
090  75  -
091  43 RCL
092  06  06
093  95  =
094  42 STO
095  10  10
096  02  2
097  00  0
098  35  1/X
099  42 STO
100  11  11
101  01  1
102  42 STO
103  12  12
104  00  0
105  42 STO
106  13  13
107  43 RCL
108  13  13
109  19  D'
110  42 STO
111  14  14
112  85  +
113  43 RCL
114  06  06
115  95  =
116  59 INT
117  99 PRT
118  43 RCL
119  14  14
120  75  -
121  43 RCL
122  10  10
123  95  =
124  32 X:T
125  01  1
126  77  GE
127  01  01
128  90  90
129  43 RCL
130  11  11
131  55  ÷
132  43 RCL
133  12  12
134  95  =
135  42 STO
136  11  11
137  43 RCL
138  13  13
139  85  +
140  43 RCL
141  11  11
142  95  =
143  42 STO
144  13  13
145  43 RCL
146  13  13
147  19  D'
148  42 STO
149  14  14
150
```

PROGRAM FOR PREDICTION OF CASE
(Three-Dimensional)

```
151  43 RCL
152  10  10
153  95  =
154  50 I×I
155  32 X:T
156  01  1
157  77  GE
158  01  01
159  90  90
160  43 RCL
161  10  10
162  32 X:T
163  43 RCL
164  14  14
165  77  GE
166  01  01
167  29  29
168  02  2
169  42 STO
170  12  12
171  43 RCL
172  11  11
173  55  ÷
174  43 RCL
175  12  12
176  95  =
177  42 STO
178  11  11
179  43 RCL
180  13  13
181  75  -
182  43 RCL
183  11  11
184  95  =
185  42 STO
186  13  13
187  61 GTO
188  01  01
189  45  45
190  58 FIX
191  04  04
192  43 RCL
193  13  13
194  99 PRT
195  55  ÷
196  02  2
197  93  .
198  05  5
199  04  4
200  65  ×
201  01  1
202  00  0
203  00  0
204  00  0
205  95  =
206  99 PRT
207  98 ADV
208  22 INV
209  58 FIX
210  43 RCL
211  09  09
212  99 PRT
213  43 RCL
214  16  16
215  99 PRT
216  98 ADV
217  54  )
218  92 RTN
219  76 LBL
220  19 D'
221  53  (
222  42 STO
223  13  13
224  55  ÷
225  02  2
226  55  ÷
227  53  (
228  43 RCL
229  03  03
230  65  ×
231  43 RCL
232  08  08
233  54  )
234  34 FX
235  95  =
236  10 E'
237  65  ×
238  02  2
239  65  ×
240  43 RCL
241  07  07
242  55  ÷
243  43 RCL
244  02  02
245  65  ×
246  53  (
247  43 RCL
248  03  03
249  65  ×
250  43 RCL
251  08  08
252  54  )
253  34 FX
254  95  =
255  42 STO
256  15  15
257  02  2
258  65  ×
259  43 RCL
260  13  13
261  55  ÷
262  43 RCL
263  05  05
264  95  =
265  42 STO
266  16  16
267  01  1
268  42 STO
269  17  17
270  04  4
271  32 X:T
272  43 RCL
273  09  09
274  77  GE
275  06  06
276  37  37
277  02  2
278  32 X:T
279  43 RCL
280  09  09
281  77  GE
282  05  05
283  32  32
284  01  1
285  32 X:T
286  43 RCL
287  09  09
288  77  GE
289  04  04
290  11  11
291  53  (
292  00  0
293  93  .
294  00  0
295  01  1
296  02  2
297  01  1
298  04  4
299  06  6
300  65  ×
```

PROGRAM FOR PREDICTION OF CASE
(Three-Dimensional)

301	43	RCL
302	09	09
303	33	X^2
304	85	+
305	00	0
306	93	.
307	00	0
308	05	5
309	06	6
310	00	0
311	06	6
312	05	5
313	65	×
314	43	RCL
315	09	09
316	85	+
317	00	0
318	93	.
319	00	0
320	06	6
321	06	6
322	06	6
323	01	1
324	54	)
325	65	×
326	43	RCL
327	16	16
328	33	X^2
329	85	+
330	53	(
331	00	0
332	93	.
333	00	0
334	02	2
335	01	1
336	08	8
337	01	1
338	04	4
339	65	×
340	43	RCL
341	09	09
342	33	X^2
343	75	-
344	00	0
345	93	.
346	00	0
347	01	1
348	04	4
349	04	4
350	03	3

351	05	5
352	65	×
353	43	RCL
354	09	09
355	75	-
356	00	0
357	93	.
358	02	2
359	08	8
360	03	3
361	01	1
362	06	6
363	01	1
364	54	)
365	65	×
366	43	RCL
367	16	16
368	85	+
369	53	(
370	00	0
371	93	.
372	00	0
373	06	6
374	05	5
375	05	5
376	01	1
377	65	×
378	43	RCL
379	09	09
380	35	1/X
381	33	X^2
382	75	-
383	00	0
384	93	.
385	03	3
386	02	2
387	08	8
388	07	7
389	07	7
390	04	4
391	65	×
392	43	RCL
393	09	09
394	35	1/X
395	85	+
396	00	0
397	93	.
398	09	9
399	07	7
400	00	0

401	02	2
402	04	4
403	07	7
404	54	)
405	95	=
406	42	STO
407	17	17
408	61	GTO
409	06	06
410	37	37
411	53	(
412	00	0
413	93	.
414	00	0
415	04	4
416	08	8
417	09	9
418	02	2
419	06	6
420	65	×
421	43	RCL
422	09	09
423	33	X^2
424	75	-
425	00	0
426	93	.
427	00	0
428	03	3
429	05	5
430	08	8
431	08	8
432	05	5
433	65	×
434	43	RCL
435	09	09
436	85	+
437	00	0
438	93	.
439	01	1
440	02	2
441	01	1
442	07	7
443	08	8
444	54	)
445	65	×
446	43	RCL
447	16	16
448	33	X^2
449	75	-
450	53	(

PROGRAM FOR PREDICTION OF CASE
(Three-Dimensional)

```
451  00   0
452  93   .
453  00   0
454  01   1
455  02   2
456  09   9
457  02   2
458  02   2
459  65   ×
460  43   RCL
461  09   09
462  33   X²
463  75   -
464  00   0
465  93   .
466  00   0
467  07   7
468  02   2
469  04   4
470  00   0
471  05   5
472  65   ×
473  43   RCL
474  09   09
475  85   +
476  00   0
477  93   .
478  03   3
479  03   3
480  05   5
481  02   2
482  06   6
483  05   5
484  54   )
485  65   ×
486  43   RCL
487  16   16
488  85   +
489  53   (
490  00   0
491  93   .
492  01   1
493  03   3
494  04   4
495  08   8
496  03   3
497  02   2
498  65   ×
499  43   RCL
500  09   09
501  35   1/X
502  33   X²
503  75   -
504  00   0
505  93   .
506  04   4
507  04   4
508  04   4
509  02   2
510  09   9
511  06   6
512  65   ×
513  43   RCL
514  09   09
515  35   1/X
516  85   +
517  01   1
518  93   .
519  00   0
520  01   1
521  06   6
522  04   4
523  06   6
524  08   8
525  54   )
526  95   =
527  42   STO
528  17   17
529  61   GTO
530  06   06
531  37   37
532  53   (
533  00   0
534  93   .
535  00   0
536  01   1
537  09   9
538  09   9
539  01   1
540  65   ×
541  43   RCL
542  09   09
543  33   X²
544  85   +
545  00   0
546  93   .
547  00   0
548  06   6
549  03   3
550  01   1
551  08   8
552  65   ×
553  43   RCL
554  09   09
555  85   +
556  00   0
557  93   .
558  00   0
559  01   1
560  01   1
561  54   )
562  65   ×
563  43   RCL
564  16   16
565  33   X²
566  75   -
567  53   (
568  00   0
569  93   .
570  00   0
571  00   0
572  05   5
573  06   6
574  08   8
575  65   ×
576  43   RCL
577  09   09
578  33   X²
579  75   -
580  00   0
581  93   .
582  00   0
583  04   4
584  08   8
585  04   4
586  65   ×
587  43   RCL
588  09   09
589  85   +
590  00   0
591  93   .
592  03   3
593  00   0
594  04   4
595  01   1
596  54   )
597  65   ×
598  43   RCL
599  16   16
600  85   +
```

PROGRAM FOR PREDICTION OF CASE
(Three-Dimensional)

```
601  53  (
602  00  0
603  93  .
604  01  1
605  01  1
606  02  2
607  03  3
608  03  3
609  65  ×
610  43  RCL
611  09  09
612  35  1/X
613  33  X²
614  75  -
615  00  0
616  93  .
617  04  4
618  04  4
619  04  4
620  01  1
621  65  ×
622  43  RCL
623  09  09
624  35  1/X
625  85  +
626  01  1
627  93  .
628  00  0
629  02  2
630  01  1
631  06  6
632  03  3
633  54  )
634  95  =
635  42  STO
636  17  17
637  43  RCL
638  15  15
639  65  ×
640  43  RCL
641  17  17
642  95  =
643  54  )
644  92  RTN
645  76  LBL
646  10  E'
647  53  (
648  42  STO
649  18  18
650  65  ×

651  00  0
652  93  .
653  03  3
654  02  2
655  07  7
656  05  5
657  09  9
658  01  1
659  01  1
660  85  +
661  01  1
662  95  =
663  35  1/X
664  42  STO
665  19  19
666  53  (
667  00  0
668  93  .
669  02  2
670  05  5
671  04  4
672  08  8
673  02  2
674  09  9
675  05  5
676  09  9
677  02  2
678  65  ×
679  43  RCL
680  19  19
681  75  -
682  00  0
683  93  .
684  02  2
685  08  8
686  04  4
687  04  4
688  09  9
689  06  6
690  07  7
691  03  3
692  06  6
693  65  ×
694  43  RCL
695  19  19
696  33  X²
697  85  +
698  01  1
699  93  .
700  04  4

701  02  2
702  01  1
703  04  4
704  01  1
705  03  3
706  07  7
707  04  4
708  01  1
709  65  ×
710  43  RCL
711  19  19
712  45  YX
713  03  3
714  75  -
715  01  1
716  93  .
717  04  4
718  05  5
719  03  3
720  01  1
721  05  5
722  02  2
723  00  0
724  02  2
725  07  7
726  65  ×
727  43  RCL
728  19  19
729  45  YX
730  04  4
731  85  +
732  01  1
733  93  .
734  00  0
735  06  6
736  01  1
737  04  4
738  00  0
739  05  5
740  04  4
741  02  2
742  09  9
743  65  ×
744  43  RCL
745  19  19
746  45  YX
747  05  5
748  54  )
749  65  ×
750  01  1
```

PROGRAM FOR PREDICTION OF CASE

(Three-Dimensional)

```
751   22 INV
752   23 LNX
753   45 Y^x
754   43 RCL
755   18  18
756   33 X²
757   94 +/-
758   95  =
759   42 STO
760   19  19
761   01  1
762   22 INV
763   23 LNX
764   45 Y^x
765   43 RCL
766   18  18
767   33 X²
768   94 +/-
769   55  ÷
770   89  π
771   34 √X
772   75  -
773   43 RCL
774   18  18
775   65  ×
776   43 RCL
777   19  19
778   95  =
779   54  )
780   92 RTN
```

END
FILMED
4-86
DTIC